A poroplastic model of structural reorganisation in porous media of biomechanical interest

Noname manuscript No.
(will be inserted by the editor)

A poroplastic model of structural reorganisation in porous media of biomechanical interest

Dedicated to Prof. David Steigmann in recognition of his contributions

Alfio Grillo · Raphael Prohl · Gabriel Wittum

Received: date / Accepted: date

DOI: 10.1007/s00161-015-0465-y. Available online: August 13, 2015
Journal: *Continuum Mechanics and Thermodynamics* (Springer)

Abstract We present a poroplastic model of structural reorganisation in a binary mixture comprising a solid and a fluid phase. The solid phase is the macroscopic representation of a deformable porous medium, which exemplifies the matrix of a biological system (consisting e.g. of cells, extra-cellular matrix, collagen fibres). The fluid occupies the interstices of the porous medium and is allowed to move throughout it. The system reorganises its internal structure in response to mechanical stimuli. Such structural reorganisation, referred to as *remodelling*, is described in terms of "plastic" distortions, whose evolution is assumed to obey a phenomenological flow rule driven by stress. We study the influence of remodelling on the mechanical and hydraulic behaviour of the system, showing how the plastic distortions modulate the flow pattern of the fluid, and the distributions of pressure and stress inside it. To accomplish this task, we solve a highly non-linear set of model equations by elaborating a previously developed numerical procedure, which is implemented in a non-commercial Finite Element solver.

A. Grillo
DISMA "G.L. Lagrange", Politecnico di Torino, C.so Duca degli Abruzzi 24, I-10129, Torino (TO) Italy
Tel.: +39-011-0907531
Fax: +39-011-0907599
E-mail: alfio.grillo@polito.it

R. Prohl
Steinbeis Center, Simulation in Technology, Bussardweg 6, D-75446 Wiernsheim, Germany.
E-mail: raphael@techsim.org

G. Wittum
G-CSC, Goethe Universität Frankfurt. Kettenhofweg 139, D-60325, Frankfurt am Main, Germany. E-mail: wittum@gcsc.uni-frankfurt.de

Keywords Mixture Theories · Porous Media · Poroplasticity · Remodelling · Soft Tissues

1 Introduction

The remodelling, or structural reorganisation, of a biological system might be defined as the result of an *ensemble* of processes that concur to adapt its structure and material properties to both internal and external stimuli. In addition to remodelling, a biological system may also experience growth, i.e., it may gain or lose mass. Growth can be appositional or volumetric. In the first case, new material is either removed or laid over the pre-existing one [12]. In the second case, instead, the variation of mass can be diverted either in a change of volume or in a change of density of the system [31, 62, 63].

In principle, a comprehensive study of growth and remodelling requires an interdisciplinary approach, in which genetic aspects and molecular processes as well as intracellular and intercellular activities are accounted for. Furthermore, a thorough analysis of the functioning of biological systems calls for multi-scale and multi-level mathematical models, which should couple chemical, electrical, and mechanical phenomena. Despite these intricacies, some essential features of the evolution of biological systems can be captured by purely mechanical theories of growth and remodelling. For a given biological system, the starring characters of such theories are the parameters describing its kinematics and structural evolution, and the generalised forces conjugate with the selected parameters. Within a purely mechanical approach, several problems of growth and remodelling can be studied. Growth, in general, contributes to change the properties and internal structure of the tissue in which it occurs. A relevant aspect of this phenomenology is that grown tissues usually feature residual stresses, which means that, even though a grown tissue finds itself in an unloaded configuration, it is not necessarily in a stress-free state. For example, this is true for arteries [52]. Thus, as suggested in [90], growth can be thought of as the process that brings the tissue from a zero-stress state to a state in which residual stresses may be present even in the absence of external loading. As is well-known, the stress-free state of a body (which is also referred to as "the natural state") is not a true configuration. Rather, it is a collection of relaxed body pieces, which cannot be attained by simply deforming the body. Consequently, growth cannot be described just in terms of deformation, deformation gradients, and the related measures of stress. In fact, one has to introduce also the concept of incompatible distortions in order to account for the transformation connecting the natural state of a tissue with the unloaded—yet not stress-free—configuration chosen as reference. The distortions due to growth are generally non-integrable and incompatible. They are said to be non-integrable when they cannot be expressed as deformation gradients, and are said to be incompatible when they lead to the loss of flatness of the body manifold [72]. Moreover, distortions are both formally and conceptually distinct from deformations, which describe the global change of shape of the tissue. To account for distortions, Rodriguez et al. [90] invoked the Bilby-Kröner-Lee (BKL) decomposition of the deformation gradient tensor, thereby separating the "elastic" part of the overall deformation from the "anelastic" one, which is related to growth and remodelling, and need not be compatible.

The use of the BKL decomposition permits to exploit several analogies with the theory of Elastoplasticity. For example, in a general model of growth, the anelastic distortions associated with the structural reorganisation of a tissue were described in terms of material inhomogeneities in [31], while the concept of "evolving natural configurations" [89] was used for modelling tumour growth both in monophasic and in multiphasic materials [1,86].

In this paper, we focus on remodelling only. This can be done because there exist remodelling processes that do not lead to variations of mass. Moreover, there exist cases in which remodelling takes place over time-scales that are well-separated from those characterising growth, and can be thus decoupled from the growth-driven evolution of the system under study. For example, these conditions are met in cellular aggregates and in tumour spheroids, when their remodelling consists of the reorganisation of the adhesion bonds among the cells [42]. This kind of remodelling can be described by hypothesising that the considered biological systems exhibit elastoplastic behaviour [4] (or, in some cases, elasto-visco-plastic behaviour [84]), and assuming that plastic distortions arise when the stress in the system exceeds a given threshold [42]. The closeness of the present setting with the classical theory of Elastoplasticity (cf. e.g. [65,71]) makes it rather natural to employ the BKL decomposition in order to define a stress-free state for the system, and separate the plastic distortions due to remodelling from the elastic part of the overall deformation gradient. Moreover, as is the case in Elastoplasticity, also in this framework the plastic distortions are generally non-integrable and incompatible. For this reason, when referring to the distortions associated with the evolution of the internal structure of a body (i.e., with the process of remodelling), we shall use the adjectives "anelastic" and "plastic" interchangeably.

Following [3,45], we consider a biphasic mixture comprising a solid and a fluid phase, and take it as an exemplification of a biological system. We study the evolution of the mixture in response to external loads by prescribing that, under suitable conditions, a remodelling process of the solid phase occurs. To accomplish this task, we formulate a finite-deformation poroplastic model of the mixture, which is able to determine the deformation of the solid phase, the velocity of the fluid phase, and the plastic distortions associated with the occurrence of remodelling. To solve the problem, we elaborate a computational algorithm that aims at generalising a well-established numerical procedure—the Return Mapping Algorithm (RMA)—to a class of anelastic models not necessarily complying with all the hypotheses on which the RMA is based [93]. Besides testing the proposed algorithm, our main purpose is to evaluate the influence of remodelling on the fluid velocity, overall deformation, and distributions of pressure and constitutive stress in the system under study.

We remark that mixture theory has been largely employed in modelling biomechanical problems of different kind. These range from tumour growth [2], in which the considered mixture consists of a fluid and one or more cell populations, to bone reconstruction [60], in which the mixture consists of the bone itself and some grafted bio-resorbable material.

The issue of structural reorganisation is largely investigated in the context of bone biomechanics, and has recently contributed also to raise questions in the field of optimal control theory. For example, optimal control procedures have been elaborated in [5] for assessing the structural efficiency of adaptive materials, and in [6] for studying the adaptation of bones under mechanical stimuli. They have also been used for modelling the trabecular architecture of bones [7], and for evaluating the bone density distribution [8]. Another problem connected with bone remodelling, which concerns the interaction of bone with resorbable biomaterial, has been addressed in [9–11].

The paper is organised as follows. In Sect. 2, we review some aspects of the theory of biphasic mixtures, and introduce the BKL decomposition in the framework of porous media. In Sect. 3, we establish the constitutive framework, study dissipation, and determine the evolution law for remodelling. In Sect. 4, we describe the numerical procedure elaborated for solving the model equations. In Sect. 5, we present and discuss the obtained results. Finally, in section 6, we outline some critical remarks on the employed model, and propose some plans for future research.

2 Theoretical background

For our purposes, we consider a binary system comprising a porous solid medium, also referred to as "matrix" hereafter, and a fluid. The region of space occupied by the system as a whole can be partitioned into two complementary sub-regions. One of these regions is occupied by the solid particles constituting the matrix, while the other one, which is generated by the voids of the matrix, is assumed to be filled with the fluid. If the latter sub-region is connected in topological sense, it is termed "pore space", and the fluid can circulate throughout it. In the following, the matrix and the fluid shall also be called "phases". At a sufficiently coarse scale of observation, the system can be viewed as a biphasic mixture, which means that both the matrix and the fluid are admitted to co-exist at each point of space occupied by the system. Note that there may be cases in which the connectedness of the void region is not granted. This happens, e.g., in solid bodies with micro-periodic non-connected inclusions filled with fluid [26].

2.1 Kinematics of biphasic mixtures

We base the forthcoming description of the kinematics of biphasic mixtures on the theory developed in [87,88], and recently summarised in [94]. We denote by

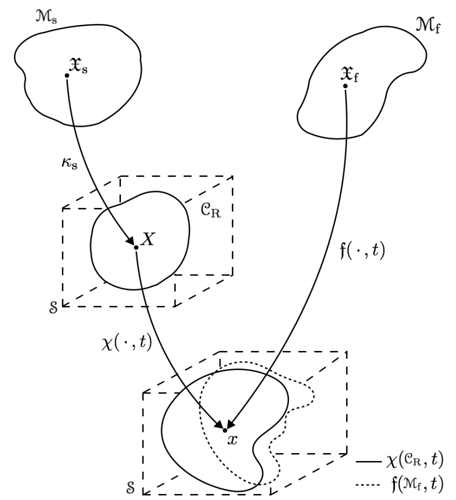

Fig. 1 Graphical representation of the kinematics of biphasic mixtures. Picture redrawn and adapted from [88]

$\mathcal{M}_{\mathrm{s}}$ and $\mathcal{M}_{\mathrm{f}}$ the two smooth three-dimensional material manifolds associated with the matrix and the fluid, respectively. The manifold $\mathcal{M}_{\mathrm{s}}$ is embedded into the three-dimensional Euclidean point space $\mathcal{S}$ by means of the smooth localisation function $\kappa_{\mathrm{s}} : \mathcal{M}_{\mathrm{s}} \to \mathcal{S}$, such that, for every solid particle $\mathfrak{X}_{\mathrm{s}} \in \mathcal{M}_{\mathrm{s}}$, there exists a reference placement $X = \kappa_{\mathrm{s}}(\mathfrak{X}_{\mathrm{s}}) \in \mathcal{S}$. The set $\mathcal{C}_{\mathrm{R}} = \kappa_{\mathrm{s}}(\mathcal{M}_{\mathrm{s}})$ is chosen as the reference configuration for the mixture. The motion of the solid constituent is the one-parameter family of smooth mappings $\chi(\,\cdot\,,t) : \mathcal{C}_{\mathrm{R}} \to \mathcal{S}$, where $t \in \mathcal{I} \subseteq \mathbb{R}$ is time and $\mathcal{I}$ is the interval of time over which the mixture is observed. The set $\chi(\mathcal{C}_{\mathrm{R}}, t) \subset \mathcal{S}$ defines the current configuration of the solid phase. Each point $x \in \chi(\mathcal{C}_{\mathrm{R}}, t) \subset \mathcal{S}$ is such that $x = \chi(X, t)$, with $X \in \mathcal{C}_{\mathrm{R}}$ and $t \in \mathcal{I}$. Similarly, the motion of the fluid is defined by $\mathfrak{f}(\,\cdot\,,t) : \mathcal{M}_{\mathrm{f}} \to \mathcal{S}$, with $t \in \mathcal{I}$. The map $\mathfrak{f}(\,\cdot\,,t)$ places a fluid particle $\mathfrak{X}_{\mathrm{f}} \in \mathcal{M}_{\mathrm{f}}$ in the spatial point $x = \mathfrak{f}(\mathfrak{X}_{\mathrm{f}}, t) \in \mathfrak{f}(\mathcal{M}_{\mathrm{f}}, t)$, where $\mathfrak{f}(\mathcal{M}_{\mathrm{f}}, t)$ is the region of $\mathcal{S}$ occupied by the fluid at time t. Therefore, at the same instant of time, the biphasic mixture occupies the set $\mathcal{C}_t = \chi\,(\kappa_{\mathrm{s}}(\mathcal{M}_{\mathrm{s}}), t) \cap \mathfrak{f}\,(\mathcal{M}_{\mathrm{f}}, t) \subset \mathcal{S}$. By construction, solid and fluid particles co-exist at each point $x \in \mathcal{C}_t$. A schematic picture of the kinematics of biphasic mixtures is reported in Fig. 1, which has been adapted from [88].

We introduce the tangent spaces attached at $x \in \mathcal{S}$ and $X \in \mathcal{C}_{\mathrm{R}}$, i.e., $T_x\mathcal{S}$ and $T_X\mathcal{C}_{\mathrm{R}}$, the tangent bundles $T\mathcal{S} := \sqcup_{x\in\mathcal{S}} T_x\mathcal{S}$ and $T\mathcal{C}_{\mathrm{R}} = \sqcup_{X\in\mathcal{C}_{\mathrm{R}}} T_X\mathcal{C}_{\mathrm{R}}$ (where $\sqcup$ stands for "disjoint union" of sets), and their dual spaces $T^*\mathcal{S}$ and $T^*\mathcal{C}_{\mathrm{R}}$, termed cotangent bundles. In addition, for any pair of natural numbers $r \geq 0$

and $s \geq 0$, we define the spaces [33]

$$[T\mathcal{S}]^r{}_s = \underbrace{T\mathcal{S} \otimes \ldots \otimes T\mathcal{S}}_{r \text{ times}} \otimes \underbrace{T^*\mathcal{S} \otimes \ldots \otimes T^*\mathcal{S}}_{s \text{ times}}, \tag{1a}$$

$$[T\mathcal{C}_{\mathrm{R}}]^r{}_s = \underbrace{T\mathcal{C}_{\mathrm{R}} \otimes \ldots \otimes T\mathcal{C}_{\mathrm{R}}}_{r \text{ times}} \otimes \underbrace{T^*\mathcal{C}_{\mathrm{R}} \otimes \ldots \otimes T^*\mathcal{C}_{\mathrm{R}}}_{s \text{ times}}. \tag{1b}$$

When r is zero, we simply write $[T\mathcal{S}]^0_s$ and $[T\mathcal{C}_{\mathrm{R}}]^0_s$. Analogously, when s is zero, we adopt the notation $[T\mathcal{S}]^r_0$ and $[T\mathcal{C}_{\mathrm{R}}]^r_0$. For the sake of generality, we adopt the covariant formalism [68]. In the forthcoming calculations, we employ the spatial metric tensor, $\boldsymbol{g} \in [T\mathcal{S}]^0_2$, and the "material" metric tensor, $\boldsymbol{G} \in [T\mathcal{C}_{\mathrm{R}}]^0_2$. Moreover, we adhere to the convention that the gradient of scalar fields returns a covector, and that all the stress tensors introduced in the following have contravariant components in their component representation.

The velocity of a solid particle, $\mathfrak{X}_{\mathrm{s}}$, passing through $x = \chi(\kappa_{\mathrm{s}}(\mathfrak{X}_{\mathrm{s}}), t)$ at time t is denoted by $\boldsymbol{v}_{\mathrm{s}}(x,t) = \dot{\chi}(\kappa_{\mathrm{s}}(\mathfrak{X}_{\mathrm{s}}), t) = \dot{\chi}(X,t) \in T_x\mathcal{S}$. Analogously, $\boldsymbol{v}_{\mathrm{f}}(x,t) = \dot{\mathfrak{f}}(\mathfrak{X}_{\mathrm{f}}, t) \in T_x\mathcal{S}$ is the spatial velocity of a fluid particle, $\mathfrak{X}_{\mathrm{f}}$, passing through $x = \mathfrak{f}(\mathfrak{X}_{\mathrm{f}}, t)$. The velocity of the fluid relative to the solid is given by $\boldsymbol{v}_{\mathrm{fs}}(x,t) = \boldsymbol{v}_{\mathrm{f}}(x,t) - \boldsymbol{v}_{\mathrm{s}}(x,t)$, with $x = \chi(\kappa_{\mathrm{s}}(\mathfrak{X}_{\mathrm{s}}), t) = \mathfrak{f}(\mathfrak{X}_{\mathrm{f}}, t)$. Moreover, the acceleration of the αth phase is defined by $\boldsymbol{a}_\alpha(x,t) = D_\alpha \boldsymbol{v}_\alpha(x,t)$, where D_α is the substantial derivative operator with respect to $\boldsymbol{v}_\alpha$, i.e.,

$$D_\alpha \boldsymbol{v}_\alpha = \partial_t \boldsymbol{v}_\alpha + (\operatorname{grad} \boldsymbol{v}_\alpha)\, \boldsymbol{v}_\alpha, \quad \alpha = \mathrm{s}, \mathrm{f}. \tag{2}$$

To express the velocity of the αth phase as a function of the points $X \in \mathcal{C}_{\mathrm{R}}$, we perform the composition $\boldsymbol{u}_\alpha(\,\cdot\,, t) = \boldsymbol{v}_\alpha(\,\cdot\,, t) \circ \chi(\,\cdot\,, t)$. However, from now on we shall omit the explicit dependence on time in the composition of functions, so that, for example, the velocity field $\boldsymbol{u}_\alpha : \mathcal{C}_{\mathrm{R}} \times \mathcal{I} \to T\mathcal{S}$ shall be simply denoted by $\boldsymbol{u}_\alpha = \boldsymbol{v}_\alpha \circ \chi$.

The tangent map of $\chi(\,\cdot\,, t)$ at $X \in \mathcal{C}_{\mathrm{R}}$ defines the deformation gradient tensor of the solid motion, $\boldsymbol{F}(X,t) = T\chi(X,t) : T_X\mathcal{C}_{\mathrm{R}} \to T_x\mathcal{S}$. In order for χ to be admissible, the condition $J = \det(\boldsymbol{F}) > 0$ must be respected at all points and all times. The transpose, inverse, and transpose inverse of $\boldsymbol{F}$ are defined as $\boldsymbol{F}^{\mathrm{T}} : T^*\mathcal{S} \to T^*\mathcal{C}_{\mathrm{R}}$, $\boldsymbol{F}^{-1} : T\mathcal{S} \to T\mathcal{C}_{\mathrm{R}}$, and $\boldsymbol{F}^{-\mathrm{T}} : T^*\mathcal{C}_{\mathrm{R}} \to T^*\mathcal{S}$, respectively. It also holds that $\boldsymbol{G}^{-1}\boldsymbol{F}^{\mathrm{T}}\boldsymbol{g} : T\mathcal{S} \to T\mathcal{C}_{\mathrm{R}}$. This combination of tensors shall be used in the definition of the Mandel stress tensors (cf. Sect. 3). The symmetric, positive definite, second-order tensor $\boldsymbol{C} = \boldsymbol{F}^{\mathrm{T}}\boldsymbol{g}\boldsymbol{F} \in [T\mathcal{C}_{\mathrm{R}}]^0_2$ is the Cauchy-Green deformation tensor induced by $\boldsymbol{F}$. For $\alpha = \mathrm{s}, \mathrm{f}$, we also introduce the spatial velocity gradient $\boldsymbol{\ell}_\alpha = (\operatorname{grad} \boldsymbol{v}_\alpha) \circ \chi \in T\mathcal{S} \otimes T^*\mathcal{S}$, which is related to the "material" velocity gradient, $\operatorname{Grad} \boldsymbol{u}_\alpha \in T\mathcal{S} \otimes T^*\mathcal{C}_{\mathrm{R}}$, through $\operatorname{Grad} \boldsymbol{u}_{\mathrm{s}} = \dot{\boldsymbol{F}} = \boldsymbol{\ell}_{\mathrm{s}}\boldsymbol{F}$ and $\operatorname{Grad} \boldsymbol{u}_{\mathrm{f}} := \boldsymbol{\ell}_{\mathrm{f}}\boldsymbol{F}$, respectively.

2.2 The Bilby-Kröner-Lee (BKL) decomposition for porous media

In this work, we study the remodelling that occurs in a biological system when, under appropriate loading conditions, the system is compelled to reorganise its internal structure in order to sustain the applied loads. In the case of cellular aggregates [42], this type of remodelling manifests itself through the structural transformation of the actin network in the cells, and the reorganisation of the adhesion bonds among the cells. In soft tissues, such as articular cartilage, the considered remodelling might represent the rearrangement of the cross-links of the fibre network forming the extracellular matrix. These processes can be described in terms of "plastic distortions" [42]. It is important to recall that this kind of remodelling is characterised by time scales (in fact, those induced by the mechanical loads) that allow to decouple it from the structural evolution ascribable to growth. Growth, indeed, is due to the mitosis and apoptosis of the cells, which typically occur over sufficiently larger time scales. For this reason, we disregard growth-related aspects of remodelling in the present framework.

To describe the deformation and the plastic distortions that accompany the remodelling of the biological system under study, we introduce, in addition to $\boldsymbol{F}$, the "tensor of plastic distortions" $\boldsymbol{F}_{\mathrm{p}}$. This leads us to the Bilby-Kröner-Lee (BKL) multiplicative decomposition $\boldsymbol{F} = \boldsymbol{F}_{\mathrm{e}}\boldsymbol{F}_{\mathrm{p}}$, where $\boldsymbol{F}_{\mathrm{e}}$ is sometimes referred to as the "accommodating part" of the overall deformation gradient tensor. To sketch the conceptual meaning of $\boldsymbol{F}_{\mathrm{p}}$, we refer to [71]. Hence, we consider a body that is brought from its reference, unloaded configuration, $\mathcal{C}_{\mathrm{R}}$, to the current configuration, $\mathcal{C}_t$, by the action of applied loads. If this evolution is accompanied by a structural reorganisation, the body cannot be brought back to $\mathcal{C}_{\mathrm{R}}$ by removing the external loads. Rather, even though all external loads were removed, the system would occupy a configuration different from $\mathcal{C}_t$ and $\mathcal{C}_{\mathrm{R}}$, in which residual stresses and residual strains may be present. To eliminate these, one should ideally tear the body to small disjoint pieces (i.e., neighbourhoods of material points), and let each of them individually attain a stress-free state (in doing this ideal tearing, time is kept fixed). The collection of all these stress-free body pieces, determined through the ideal tearing process, is said to be the "natural state" of the body at time t. The plastic distortion $\boldsymbol{F}_{\mathrm{p}}$ is the distortion that has to be applied to the material neighbourhoods of the points in $\mathcal{C}_{\mathrm{R}}$ to obtain the body pieces collected in the natural state. If the material shows elastic behaviour from its natural state, the accommodating distortion, $\boldsymbol{F}_{\mathrm{e}}$, is the elastic distortion that has to be applied to the body elements in the natural state to retrieve the global configuration $\mathcal{C}_t$. The BKL decomposition can be understood as a combination of "tangent bundle maps" [83], so that one can introduce a time-dependent intermediate map $\chi_\kappa(\,\cdot\,,t) : \mathcal{C}_{\mathrm{R}} \to \mathcal{S}$, which constitutes the base map for $\boldsymbol{F}_{\mathrm{p}}$. However, the existence of $\chi_\kappa(\,\cdot\,,t)$ does not necessarily imply that $\boldsymbol{F}_{\mathrm{p}}$ is the tangent map of $\chi_\kappa(\,\cdot\,,t)$. In fact, in general, $\boldsymbol{F}_{\mathrm{p}}$ is neither compatible nor integrable, i.e., there exists no deformation whose tangent map equals $\boldsymbol{F}_{\mathrm{p}}$. In the following, we call the set $\chi_\kappa(\mathcal{C}_{\mathrm{R}}, t) = \mathcal{C}_\kappa \subset \mathcal{S}$ "intermediate configuration" (cf. Fig. 2), and associate it with the "natural state" of the solid phase.

Due to the BKL decomposition, the velocity gradient of the solid phase, $\boldsymbol{\ell}_{\mathrm{s}} = \dot{\boldsymbol{F}}\boldsymbol{F}^{-1}$, can be written as

$$\boldsymbol{\ell}_{\mathrm{s}} = \boldsymbol{\ell}_{\mathrm{e}} + \boldsymbol{\ell}_{\mathrm{p}} = \boldsymbol{\ell}_{\mathrm{e}} + \boldsymbol{F}_{\mathrm{e}}\boldsymbol{L}_{\mathrm{p}}\boldsymbol{F}_{\mathrm{e}}^{-1}\,, \tag{3}$$

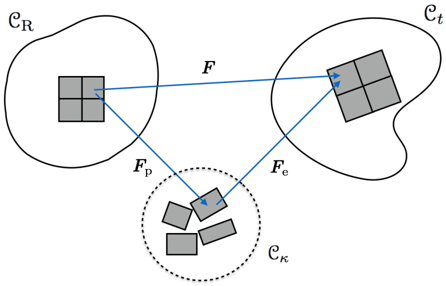

Fig. 2 Schematic representation of the BKL decomposition of the deformation gradient tensor $\boldsymbol{F}$

where $\boldsymbol{\ell}_{\mathrm{e}} = \dot{\boldsymbol{F}}_{\mathrm{e}}\boldsymbol{F}_{\mathrm{e}}^{-1}$ is the rate of elastic distortions, while $\boldsymbol{\ell}_{\mathrm{p}} = \boldsymbol{F}_{\mathrm{e}}\boldsymbol{L}_{\mathrm{p}}\boldsymbol{F}_{\mathrm{e}}^{-1}$ and $\boldsymbol{L}_{\mathrm{p}} = \dot{\boldsymbol{F}}_{\mathrm{p}}\boldsymbol{F}_{\mathrm{p}}^{-1}$ are the rates of anelastic distortions associated with the current configuration and the natural state of the system, respectively. The BKL decomposition implies the identity $J = J_{\mathrm{e}}J_{\mathrm{p}}$, where $J_{\mathrm{e}} := \det(\boldsymbol{F}_{\mathrm{e}}) > 0$ and $J_{\mathrm{p}} := \det(\boldsymbol{F}_{\mathrm{p}}) > 0$ are referred to as the elastic and anelastic volumetric ratios, respectively. The rates $\dot{J}_{\mathrm{e}}$ and $\dot{J}_{\mathrm{p}}$ can be computed as $\dot{J}_{\mathrm{e}} = J_{\mathrm{e}}\mathrm{tr}(\boldsymbol{\ell}_{\mathrm{e}})$ and $\dot{J}_{\mathrm{p}} = J_{\mathrm{p}}\mathrm{tr}(\boldsymbol{L}_{\mathrm{p}}) = J_{\mathrm{p}}\mathrm{tr}(\boldsymbol{\ell}_{\mathrm{p}})$. In the following, we shall assume that the anelastic distortions related to remodelling are volume-preserving, thereby leading to the constraint $J_{\mathrm{p}} = \det(\boldsymbol{F}_{\mathrm{p}}) = 1$, which implies $\mathrm{tr}(\boldsymbol{\ell}_{\mathrm{p}}) = 0$ and $\mathrm{tr}(\boldsymbol{L}_{\mathrm{p}}) = 0$.

For future use, we introduce $\boldsymbol{\eta}$, i.e., the metric tensor associated with the intermediate configuration $\mathcal{C}_\kappa$, and $\boldsymbol{B}_{\mathrm{p}} := \boldsymbol{C}_{\mathrm{p}}^{-1}$, where $\boldsymbol{C}_{\mathrm{p}} = \boldsymbol{F}_{\mathrm{p}}^{\mathrm{T}}\boldsymbol{\eta}\boldsymbol{F}_{\mathrm{p}}$ is the anelastic Cauchy-Green deformation tensor. Moreover, we shall exploit the kinematic identity

$$\tfrac{1}{2}\dot{\boldsymbol{B}}_{\mathrm{p}} = -\boldsymbol{F}_{\mathrm{p}}^{-1}\left(\boldsymbol{\eta}^{-1}\boldsymbol{D}_{\mathrm{p}}\boldsymbol{\eta}^{-1}\right)\boldsymbol{F}_{\mathrm{p}}^{-\mathrm{T}}\,, \tag{4}$$

where $\boldsymbol{D}_{\mathrm{p}} := \mathrm{sym}(\boldsymbol{\eta}\boldsymbol{L}_{\mathrm{p}})$.

2.3 Dynamics of biphasic mixtures

In the absence of external body forces, growth, and mass exchange processes between the solid and the fluid phase, the local forms of the mass and linear momentum balance laws for the αth phase of the biphasic mixture ($\alpha = \mathrm{s}, \mathrm{f}$) can be written as

$$\partial_t(\phi_\alpha\varrho_\alpha) + \mathrm{div}(\phi_\alpha\varrho_\alpha\boldsymbol{v}_\alpha) = 0, \qquad \text{in } \mathcal{C}_t \times \mathcal{I}\,, \tag{5a}$$

$$\phi_\alpha\varrho_\alpha\boldsymbol{a}_\alpha = \mathrm{div}\,\boldsymbol{\sigma}_\alpha + \boldsymbol{m}_\alpha, \qquad \text{in } \mathcal{C}_t \times \mathcal{I}\,, \tag{5b}$$

$$\boldsymbol{m}_{\mathrm{s}} + \boldsymbol{m}_{\mathrm{f}} = \boldsymbol{0}, \qquad \text{in } \mathcal{C}_t \times \mathcal{I}\,. \tag{5c}$$

In (5), ϕ_α and ϱ_α denote, respectively, the volumetric fraction and the true mass density of the αth phase, $\boldsymbol{\sigma}_\alpha$ is the Cauchy stress tensor, and $\boldsymbol{m}_\alpha$ is the rate of linear momentum exchange between the αth phase and the other one. Equation (5c) expresses that the mixture is closed with respect to linear momentum.

If we assume that the pore space of the matrix is completely filled with the fluid, the volumetric fractions ϕ_{s} and ϕ_{f} are constrained by the saturation condition $\phi_{\mathrm{s}}+\phi_{\mathrm{f}}=1$, which has to be respected at all times and at all points of the mixture. In the following, ϱ_{s} and ϱ_{f} shall be assumed to be given constants. Moreover, it will be hypothesised that the inertial terms $\phi_\alpha \varrho_\alpha \boldsymbol{a}_\alpha$ are negligible. This latter hypothesis leads to a quasi-static formulation of the problem, in which the only sources of time evolution for the system are provided by time-varying boundary conditions, a (slowly) time-evolving deformation, and the presence of the time-dependent reorganisation of the tissue's internal structure. By accounting for (5c), and summing (5b) over $\alpha = \mathrm{s}, \mathrm{f}$, we obtain

$$\operatorname{div}(\boldsymbol{\sigma}_{\mathrm{s}} + \boldsymbol{\sigma}_{\mathrm{f}}) = \boldsymbol{0}\,, \qquad \text{in } \mathcal{C}_t \times \mathcal{I}\,, \tag{6a}$$

$$\operatorname{div} \boldsymbol{\sigma}_{\mathrm{f}} + \boldsymbol{m}_{\mathrm{f}} = \boldsymbol{0}\,, \qquad \text{in } \mathcal{C}_t \times \mathcal{I}\,. \tag{6b}$$

Transforming (5a) by the backward Piola-transformation induced by the solid motion $\chi(\,\cdot\,,t)$, and writing the transformed equation once for $\alpha = \mathrm{s}$ and once for $\alpha = \mathrm{f}$, it is possible to show that, after some manipulations, the mass balance laws for the solid and the fluid phase reduce to [44,45]

$$\phi_{\mathrm{s}}(\chi_{\mathrm{s}}(X,t),t) = \frac{\phi_{\mathrm{sR}}(X)}{J(X,t)}\,, \qquad \text{in } \mathcal{C}_{\mathrm{R}} \times \mathcal{I}\,, \tag{7a}$$

$$\dot{J} + \operatorname{Div}\left[(J - \phi_{\mathrm{sR}})\boldsymbol{F}^{-1}\boldsymbol{u}_{\mathrm{fs}}\right] = 0, \qquad \text{in } \mathcal{C}_{\mathrm{R}} \times \mathcal{I}\,, \tag{7b}$$

with $\boldsymbol{u}_{\mathrm{fs}} = \boldsymbol{u}_{\mathrm{f}} - \boldsymbol{u}_{\mathrm{s}} = \boldsymbol{v}_{\mathrm{fs}} \circ \chi$. In (7a), $\phi_{\mathrm{sR}}(X)$ represents the volumetric fraction of the solid phase in the reference configuration. Since ϕ_{sR} does not depend on time in the present framework, it can be chosen as a referential value for ϕ_{s}. We remark that, in the presence of growth, or in the case of non-isochoric plastic distortions, the condition $J_{\mathrm{p}} = 1$ does not necessarily apply, which means that ϕ_{sR} is not time-independent in general. Rather, in the presence of density-preserving growth [62,63], it can only be inferred that the volumetric fraction associated with the intermediate configuration, i.e., $\phi_{\mathrm{sn}}(X) := J_{\mathrm{e}}(X,t)\phi_{\mathrm{s}}(\chi(X,t),t)$, is constant in time.

3 Constitutive framework and remodelling law

If the solid phase exhibits hyperelastic material behaviour from its natural state, and if the fluid phase can be regarded as macroscopically inviscid, then admissible expressions of the Cauchy stresses $\boldsymbol{\sigma}_{\mathrm{s}}$ and $\boldsymbol{\sigma}_{\mathrm{f}}$ are given by

$$\boldsymbol{\sigma}_{\mathrm{s}} = -\phi_{\mathrm{s}} p\, \boldsymbol{g}^{-1} + \boldsymbol{\sigma}_{\mathrm{sc}}\,, \tag{8a}$$

$$\boldsymbol{\sigma}_{\mathrm{f}} = -\phi_{\mathrm{f}} p\, \boldsymbol{g}^{-1}\,, \tag{8b}$$

where $\boldsymbol{\sigma}_{\rm sc}$ is the constitutive part of the Cauchy stress associated with the solid phase, i.e.,

$$\boldsymbol{\sigma}_{\rm sc} \circ \chi = \frac{1}{J_{\rm e}} \boldsymbol{F}_{\rm e} \left(2 \frac{\partial \hat{W}_{{\rm s}\kappa}}{\partial \boldsymbol{C}_{\rm e}} (\boldsymbol{C}_{\rm e}) \right) \boldsymbol{F}_{\rm e}^{\rm T} \, . \tag{9}$$

In (9), $\hat{W}_{{\rm s}\kappa}$ is the strain energy density function of the solid phase, expressed per unit volume of the intermediate configuration, and $\boldsymbol{C}_{\rm e} = \boldsymbol{F}_{\rm p}^{-{\rm T}} \boldsymbol{C} \boldsymbol{F}_{\rm p}^{-1}$ is the elastic Cauchy-Green deformation tensor. In this work, we assume that $\hat{W}_{{\rm s}\kappa}$ is of the Holmes-Mow type [57], i.e.,

$$\hat{W}_{{\rm s}\kappa}(\boldsymbol{C}_{\rm e}) = \alpha_0 \left\{ \exp\left(\Psi(\boldsymbol{C}_{\rm e}) \right) - 1 \right\} \, , \tag{10a}$$

$$\Psi(\boldsymbol{C}_{\rm e}) = \alpha_1 [\hat{I}_1(\boldsymbol{C}_{\rm e}) - 3] + \alpha_2 [\hat{I}_2(\boldsymbol{C}_{\rm e}) - 3] - \beta \log[\hat{I}_3(\boldsymbol{C}_{\rm e})] \, , \tag{10b}$$

where α_0, α_1, α_2, and β are model parameters, while $\hat{I}_1$, $\hat{I}_2$, and $\hat{I}_3$ are the invariants of $\boldsymbol{C}_{\rm e}$, i.e.,

$$I_1 = \hat{I}_1(\boldsymbol{C}_{\rm e}) = {\rm tr}(\boldsymbol{\eta}^{-1} \boldsymbol{C}_{\rm e}) = {\rm tr}(\boldsymbol{B}_{\rm p} \boldsymbol{C}) \, , \tag{11a}$$

$$I_2 = \hat{I}_2(\boldsymbol{C}_{\rm e}) = \tfrac{1}{2} \big\{ [I_1(\boldsymbol{C}_{\rm e})]^2 - {\rm tr}[(\boldsymbol{\eta}^{-1} \boldsymbol{C}_{\rm e})^2] \big\} = \tfrac{1}{2} \left\{ I_1^2 - {\rm tr}[(\boldsymbol{B}_{\rm p} \boldsymbol{C})^2] \right\} \, , \tag{11b}$$

$$I_3 = \hat{I}_3(\boldsymbol{C}_{\rm e}) = \det(\boldsymbol{C}_{\rm e}) = J_{\rm e}^2 = J^2 \, , \tag{11c}$$

where the last equality in (11c) is due to the hypothesis of isochoric plastic distortions, i.e., $J_{\rm p} = 1$. The strain energy density function $\hat{W}_{{\rm s}\kappa}$ describes a material exhibiting isotropic elastic properties with respect to the natural state. In general, if the model of the considered tissue is inhomogeneous, the parameters α_0, α_1, α_2, and β depend on material points. Sometimes, however, for computational simplicity, or because of lack of experimental data, it is assumed that only one of these parameters is variable. For instance, in modelling articular cartilage [46], α_0 was expressed by fitting experimental data taken from the literature as a third-order polynomial function of the axial coordinate parameterising the depth of a cylindrical specimen of tissue, whereas all the other material parameters were assumed to be constant.

The expressions of $\boldsymbol{\sigma}_{\rm s}$ and $\boldsymbol{\sigma}_{\rm f}$ reported in (8a) and (8b) can be found in many works based on Mixture Theory (cf. e.g. [25,81,91]). Here, they have been adapted from [15,56] to the case of an incompressible, single-constituent fluid phase, as previously done in [34,35,45,94]. By substituting (8a) and (8b) into (6a) and (6b), the momentum balance laws for the mixture as a whole and for the fluid phase become [56]

$$\operatorname{div}(-p \, \boldsymbol{g}^{-1} + \boldsymbol{\sigma}_{\rm sc}) = \boldsymbol{0} \, , \qquad \text{in } \mathcal{C}_t \times \mathcal{I} \, , \tag{12a}$$

$$-\, \boldsymbol{g}^{-1} \left(\phi_{\rm f} {\rm grad}\, p \right) + \big(\boldsymbol{m}_{\rm f} - p \, \boldsymbol{g}^{-1} {\rm grad}\, \phi_{\rm f} \big) = \boldsymbol{0} \, , \qquad \text{in } \mathcal{C}_t \times \mathcal{I} \, . \tag{12b}$$

To determine the material form of the momentum balance law for the mixture as whole, i.e., the material counterpart of (12a), we introduce the first Piola-Kirchhoff stress tensors

$$\boldsymbol{P}_{\rm s} = J \boldsymbol{\sigma}_{\rm s} \boldsymbol{F}^{-{\rm T}} = -\phi_{\rm sR} p \, \boldsymbol{g}^{-1} \boldsymbol{F}^{-{\rm T}} + \boldsymbol{P}_{\rm sc} \, , \tag{13a}$$

$$\boldsymbol{P}_{\rm f} = J \boldsymbol{\sigma}_{\rm f} \boldsymbol{F}^{-{\rm T}} = -(J - \phi_{\rm sR}) p \, \boldsymbol{g}^{-1} \boldsymbol{F}^{-{\rm T}} \, , \tag{13b}$$

where $\boldsymbol{P}_{\mathrm{sc}} = J\boldsymbol{\sigma}_{\mathrm{sc}}\boldsymbol{F}^{-\mathrm{T}}$ is the constitutive part of $\boldsymbol{P}_{\mathrm{s}}$, and perform the Piola-transformation of (12a), i.e.,

$$\mathrm{Div}\left(-Jp\,\boldsymbol{g}^{-1}\boldsymbol{F}^{-\mathrm{T}} + \boldsymbol{P}_{\mathrm{sc}}\right) = \boldsymbol{0}, \qquad \text{in } \mathcal{C}_{\mathrm{R}} \times \mathcal{I}. \tag{14}$$

By adopting the strain energy density function $\hat{W}_{\mathrm{s}\kappa}$ specified in (10a) and (10b), $\boldsymbol{P}_{\mathrm{sc}}$ can be expressed constitutively as a function of $\boldsymbol{F}$ and $\boldsymbol{B}_{\mathrm{p}}$, i.e.,

$$\begin{aligned}\boldsymbol{P}_{\mathrm{sc}} = \hat{\boldsymbol{P}}_{\mathrm{sc}}(\boldsymbol{F},\boldsymbol{B}_{\mathrm{p}}) = 2b_1\boldsymbol{F}\boldsymbol{B}_{\mathrm{p}} + 2b_2\left(I_1\boldsymbol{F}\boldsymbol{B}_{\mathrm{p}} - \boldsymbol{F}\boldsymbol{B}_{\mathrm{p}}\boldsymbol{C}\boldsymbol{B}_{\mathrm{p}}\right)\\ + 2b_3 I_3\boldsymbol{g}^{-1}\boldsymbol{F}^{-\mathrm{T}}\,,\end{aligned} \tag{15}$$

where $b_i = \hat{b}_i(\boldsymbol{F},\boldsymbol{B}_{\mathrm{p}}) = \frac{\partial \hat{W}_{\mathrm{s}\kappa}}{\partial I_i}(\boldsymbol{F},\boldsymbol{B}_{\mathrm{p}})$, $i = 1, 2, 3$, are constitutive functions of the invariants of $\boldsymbol{C}_{\mathrm{e}}$, and can be thus written as functions of $\boldsymbol{F}$ and $\boldsymbol{B}_{\mathrm{p}}$. Hence, the overall stress $\boldsymbol{P} := \boldsymbol{P}_{\mathrm{s}} + \boldsymbol{P}_{\mathrm{f}}$, which has to be substituted into (14), reads

$$\boldsymbol{P} = \hat{\boldsymbol{P}}(p,\boldsymbol{F},\boldsymbol{B}_{\mathrm{p}}) = -Jp\,\boldsymbol{g}^{-1}\boldsymbol{F}^{-\mathrm{T}} + \hat{\boldsymbol{P}}_{\mathrm{sc}}(\boldsymbol{F},\boldsymbol{B}_{\mathrm{p}}). \tag{16}$$

For future use, we also introduce the Kirchhoff stress tensor $\boldsymbol{\tau} = \boldsymbol{P}\boldsymbol{F}^{\mathrm{T}}$ and the Mandel stress tensor $\boldsymbol{\Sigma} = \boldsymbol{G}^{-1}\boldsymbol{F}^{\mathrm{T}}\boldsymbol{g}\boldsymbol{\tau}\boldsymbol{F}^{-\mathrm{T}}$, i.e.,

$$\boldsymbol{\tau} = \hat{\boldsymbol{\tau}}(p,\boldsymbol{F},\boldsymbol{B}_{\mathrm{p}}) = -Jp\,\boldsymbol{g}^{-1} + \hat{\boldsymbol{\tau}}_{\mathrm{sc}}(\boldsymbol{F},\boldsymbol{B}_{\mathrm{p}})\,, \tag{17a}$$

$$\boldsymbol{\Sigma} = \hat{\boldsymbol{\Sigma}}(p,\boldsymbol{F},\boldsymbol{B}_{\mathrm{p}}) = -Jp\,\boldsymbol{G}^{-1} + \hat{\boldsymbol{\Sigma}}_{\mathrm{sc}}(\boldsymbol{F},\boldsymbol{B}_{\mathrm{p}})\,. \tag{17b}$$

In (17a) and (17b), the constitutive parts of $\boldsymbol{\tau}$ and $\boldsymbol{\Sigma}$, given by $\boldsymbol{\tau}_{\mathrm{sc}} = \hat{\boldsymbol{\tau}}_{\mathrm{sc}}(\boldsymbol{F},\boldsymbol{B}_{\mathrm{p}})$ and $\boldsymbol{\Sigma}_{\mathrm{sc}} = \hat{\boldsymbol{\Sigma}}_{\mathrm{sc}}(\boldsymbol{F},\boldsymbol{B}_{\mathrm{p}})$, respectively, read

$$\begin{aligned}\boldsymbol{\tau}_{\mathrm{sc}} = \hat{\boldsymbol{\tau}}_{\mathrm{sc}}(\boldsymbol{F},\boldsymbol{B}_{\mathrm{p}}) =& (2b_1 + 2b_2 I_1)\boldsymbol{F}\boldsymbol{B}_{\mathrm{p}}\boldsymbol{F}^{\mathrm{T}} - 2b_2\boldsymbol{F}\boldsymbol{B}_{\mathrm{p}}\boldsymbol{C}\boldsymbol{B}_{\mathrm{p}}\boldsymbol{F}^{\mathrm{T}}\\ &+ 2b_3 I_3\boldsymbol{g}^{-1}\,,\end{aligned} \tag{18a}$$

$$\begin{aligned}\boldsymbol{\Sigma}_{\mathrm{sc}} = \hat{\boldsymbol{\Sigma}}_{\mathrm{sc}}(\boldsymbol{F},\boldsymbol{B}_{\mathrm{p}}) =& (2b_1 + 2b_2 I_1)\boldsymbol{G}^{-1}\boldsymbol{C}\boldsymbol{B}_{\mathrm{p}} - 2b_2\boldsymbol{G}^{-1}\boldsymbol{C}\boldsymbol{B}_{\mathrm{p}}\boldsymbol{C}\boldsymbol{B}_{\mathrm{p}}\\ &+ 2b_3 I_3\boldsymbol{G}^{-1}\,.\end{aligned} \tag{18b}$$

We remark that, although $\boldsymbol{\Sigma}_{\mathrm{sc}}$ is not symmetric in general, the assumption of isotropic hyperelastic response of the solid phase, which leads to (18b), implies the symmetry conditions [69]

$$\boldsymbol{B}_{\mathrm{p}}\boldsymbol{G}\boldsymbol{\Sigma}_{\mathrm{sc}} = (\boldsymbol{B}_{\mathrm{p}}\boldsymbol{G}\boldsymbol{\Sigma}_{\mathrm{sc}})^{\mathrm{T}}\,, \tag{19a}$$

$$\boldsymbol{G}\boldsymbol{\Sigma}_{\mathrm{sc}}\boldsymbol{B}_{\mathrm{p}}^{-1} = (\boldsymbol{G}\boldsymbol{\Sigma}_{\mathrm{sc}}\boldsymbol{B}_{\mathrm{p}}^{-1})^{\mathrm{T}}\,. \tag{19b}$$

3.1 Dissipation inequality

The local form of the dissipation inequality characterising the biphasic system under investigation can be written as follows

$$D_{\mathrm{m}} = -\left\{\boldsymbol{m}_{\mathrm{f}} - p\,\boldsymbol{g}^{-1}\mathrm{grad}\,\phi_{\mathrm{f}}\right\}.\boldsymbol{v}_{\mathrm{fs}} + \boldsymbol{\sigma}_{\mathrm{sc}} : \boldsymbol{g}\boldsymbol{\ell}_{\mathrm{p}} \geq 0\,, \tag{20}$$

where D_{m} is the dissipation function of the mixture as a whole, written per unit volume of $\mathcal{C}_t$ (cf. [15,44,56] for details). Note that, more rigorously, and for consistency with (3), we should write $\boldsymbol{\sigma}_{\mathrm{sc}} : \boldsymbol{g}(\boldsymbol{\ell}_{\mathrm{p}} \circ \chi^{-1})$ in (20). However, for the sake of a lighter notation, we shall omit the composition of maps in the forthcoming calculations. Since $\boldsymbol{\ell}_{\mathrm{p}}$ has vanishing trace, only the deviatoric part of $\boldsymbol{\sigma}_{\mathrm{sc}}$ contributes to the dissipation D_{m}. Following [15,56,94], $\boldsymbol{m}_{\mathrm{f}}$ can be written as

$$\boldsymbol{m}_{\mathrm{f}} = \boldsymbol{m}_{\mathrm{fd}} + p\,\boldsymbol{g}^{-1}\mathrm{grad}\,\phi_{\mathrm{f}}\,, \tag{21}$$

where $\boldsymbol{m}_{\mathrm{fd}}$ and $p\,\boldsymbol{g}^{-1}\mathrm{grad}\phi_{\mathrm{f}}$ represent, respectively, the dissipative and the non-dissipative contribution to $\boldsymbol{m}_{\mathrm{f}}$. By substituting (21) into (12b), we obtain

$$\boldsymbol{m}_{\mathrm{fd}} = \boldsymbol{g}^{-1}\left(\phi_{\mathrm{f}}\mathrm{grad}\,p\right)\,. \tag{22}$$

Moreover, the dissipation inequality (20) takes on the form

$$D_{\mathrm{m}} = D_{\mathrm{flow}} + D_{\mathrm{rem}} = \underbrace{-\boldsymbol{m}_{\mathrm{fd}}.\boldsymbol{v}_{\mathrm{fs}}}_{D_{\mathrm{flow}}} + \underbrace{\boldsymbol{\sigma}_{\mathrm{sc}} : \boldsymbol{g}\boldsymbol{\ell}_{\mathrm{p}}}_{D_{\mathrm{rem}}} \geq 0\,. \tag{23}$$

The inequality (23) states that, within a purely mechanical framework, the only two sources of dissipation for the considered biphasic system are given by $D_{\mathrm{flow}} := -\boldsymbol{m}_{\mathrm{fd}}.\boldsymbol{v}_{\mathrm{fs}}$, i.e., the power expended by the dissipative force $\boldsymbol{m}_{\mathrm{fd}}$, which is power-conjugate with the relative velocity $\boldsymbol{v}_{\mathrm{fs}}$, and by $D_{\mathrm{rem}} := \boldsymbol{\sigma}_{\mathrm{sc}} : \boldsymbol{g}\boldsymbol{\ell}_{\mathrm{p}}$, i.e., the power expended to trigger the evolution of the internal structure of the solid phase.

3.1.1 Darcy's law

We assume that the dissipative force $\boldsymbol{m}_{\mathrm{fd}}$ can be expressed constitutively as a linear function of the filtration velocity $\boldsymbol{q} := \phi_{\mathrm{f}}\boldsymbol{v}_{\mathrm{fs}}$ [14], i.e.,

$$\boldsymbol{m}_{\mathrm{fd}} = -\boldsymbol{g}^{-1}\boldsymbol{r}\,\phi_{\mathrm{f}}\boldsymbol{v}_{\mathrm{fs}}\,, \tag{24}$$

where $\boldsymbol{r} \in [T\mathcal{S}]^0_2$ is the tensor describing the resistivity of the porous medium to fluid flow [56]. By substituting (24) into (23), the following expression of dissipation is obtained

$$D_{\mathrm{m}} = D_{\mathrm{flow}} + D_{\mathrm{rem}} = \underbrace{\mathrm{sym}(\boldsymbol{r}) : \phi_{\mathrm{f}}\left(\boldsymbol{v}_{\mathrm{fs}} \otimes \boldsymbol{v}_{\mathrm{fs}}\right)}_{D_{\mathrm{flow}}} + \underbrace{\boldsymbol{\sigma}_{\mathrm{sc}} : \boldsymbol{g}\boldsymbol{\ell}_{\mathrm{p}}}_{D_{\mathrm{rem}}} \geq 0\,, \tag{25}$$

where $\mathrm{sym}(\boldsymbol{r})$ is the symmetric part of $\boldsymbol{r}$. A direct consequence of (25) is that, if $\mathrm{sym}(\boldsymbol{r})$ is positive semi-definite, D_{flow} is always non-negative, i.e., $D_{\mathrm{flow}} \geq 0$, for any possible realisation of the relative velocity $\boldsymbol{v}_{\mathrm{fs}}$. Typically, the resistivity tensor $\boldsymbol{r}$ is assumed to be symmetric and positive definite, so that $\boldsymbol{m}_{\mathrm{fd}}$ vanishes if, and only if, $\boldsymbol{v}_{\mathrm{fs}}$ is null. Under these assumptions, and the further hypothesis that $\boldsymbol{m}_{\mathrm{fd}}$ is linear in $\boldsymbol{v}_{\mathrm{fs}}$, the standard form of Darcy's law is obtained. Indeed, by substituting (24) into (22), and solving for $\phi_{\mathrm{f}}\boldsymbol{v}_{\mathrm{fs}}$, the filtration velocity is found to be

$$\boldsymbol{q} = \phi_{\mathrm{f}}\boldsymbol{v}_{\mathrm{fs}} = -\boldsymbol{k}\,\mathrm{grad}\,p\,, \tag{26}$$

where $\boldsymbol{k} = \phi_\mathrm{f}\, \boldsymbol{r}^{-1} \in [T\mathcal{S}]^2_0$ is the hydraulic conductivity tensor of the system.

By performing a Piola transformation of (26), we obtain the material form of Darcy's law:

$$J\boldsymbol{F}^{-1}(\phi_\mathrm{f}\boldsymbol{u}_\mathrm{fs}) = (J - \phi_\mathrm{sR})\boldsymbol{F}^{-1}\boldsymbol{u}_\mathrm{fs} = -\boldsymbol{K}\,\mathrm{Grad}\, p\,. \tag{27}$$

The material second-order tensor $\boldsymbol{K} = J\boldsymbol{F}^{-1}\boldsymbol{k}\boldsymbol{F}^{-\mathrm{T}}$ is the material hydraulic conductivity tensor, and is determined by means of the Piola transformation of $\boldsymbol{k}$ with respect to the solid motion. Substituting (27) into (7b) yields

$$\dot{J} - \mathrm{Div}\,[\boldsymbol{K}\,\mathrm{Grad}\, p] = 0\,. \tag{28}$$

The constitutive law defining the hydraulic conductivity, $\boldsymbol{k}$, should comply with the material symmetries of the considered tissue (e.g., isotropy, transverse isotropy, or orthotropy). Recently, a review on several constitutive laws expressing $\boldsymbol{k}$ as a function of the tissue deformation has been given in [13]. An expression of $\boldsymbol{k}$ suitable for articular cartilage was determined by employing upscaling arguments in the small deformation regime [36, 37], and subsequently adapted to the finite-deformation framework in [34, 35, 94]. If the hydraulic response of the mixture is isotropic, and the hypothesis is made that the isotropy of the hydraulic conductivity does not change with the deformation, the tensors $\boldsymbol{k}$ and $\boldsymbol{K}$ can be expressed constitutively as

$$\boldsymbol{k} = \hat{\boldsymbol{k}}(J) = \hat{k}_0(J)\boldsymbol{g}^{-1}\,, \tag{29a}$$

$$\boldsymbol{K} = \hat{\boldsymbol{K}}(\boldsymbol{F}) = J\hat{k}_0(J)\boldsymbol{C}^{-1}\,, \tag{29b}$$

where the scalar hydraulic conductivity function $\hat{k}_0$ is given by

$$\hat{k}_0(J) = k_{0\mathrm{R}} \left(\frac{J - \phi_\mathrm{sR}}{1 - \phi_\mathrm{sR}}\right)^{m_0} \exp\left[\frac{m_1}{2}(J^2 - 1)\right]\,, \tag{30}$$

and m_0 and m_1 are material parameters [57]. According to (29a) and (30), the deformation influences the hydraulic conductivity through the volumetric ratio J only. When the condition $J = 1$ is met, the identity $\hat{k}_0(1) = k_{0\mathrm{R}}$ is obtained, which means that the scalar hydraulic conductivity becomes equal to the referential one, $k_{0\mathrm{R}}$. In general, $k_{0\mathrm{R}}$, m_0, and m_1 depend on material points. The constitutive choice of the hydraulic conductivity tensor permits to express D_flow constitutively as

$$D_\mathrm{flow} = \hat{D}_\mathrm{flow}(J, \mathrm{grad}\, p) = \hat{\boldsymbol{k}}(J) : \mathrm{grad}\, p \otimes \mathrm{grad}\, p \geq 0\,, \tag{31}$$

with $\hat{D}_\mathrm{flow}$ being quadratic in $\mathrm{grad}\, p$, and highly non-linear in J.

3.1.2 Law of remodelling

In this section, we introduce the fundamental hypotheses that lead to the law of remodelling adopted in our work. We recall that, as announced in Sect. 2.2, we are considering a type of structural evolution that can be interpreted in terms of isochoric plastic distortions. Therefore, the first hypothesis is that $\boldsymbol{F}_{\mathrm{p}}$ is restricted by the constraint $J_{\mathrm{p}} = \det(\boldsymbol{F}_{\mathrm{p}}) = 1$. This implies that the rates of plastic distortions, $\boldsymbol{\ell}_{\mathrm{p}}$ or $\boldsymbol{L}_{\mathrm{p}}$, are deviatoric, i.e., $\mathrm{tr}(\boldsymbol{\ell}_{\mathrm{p}}) = 0$, and $\mathrm{tr}(\boldsymbol{L}_{\mathrm{p}}) = 0$. A direct consequence of these facts is that the part of the dissipation function related to remodelling, i.e., D_{rem}, can be written as

$$D_{\mathrm{rem}} = \boldsymbol{\sigma}_{\mathrm{sc}} : \boldsymbol{g}\boldsymbol{\ell}_{\mathrm{p}} = J_{\mathrm{e}}^{-1}\boldsymbol{\Sigma}_{\mathrm{sc}\kappa} : \boldsymbol{\eta}\boldsymbol{L}_{\mathrm{p}} \geq 0\,. \tag{32}$$

The tensor $\boldsymbol{\Sigma}_{\mathrm{sc}\kappa} := J_{\mathrm{e}}\boldsymbol{\eta}^{-1}\boldsymbol{F}_{\mathrm{e}}^{\mathrm{T}}\boldsymbol{g}\boldsymbol{\sigma}_{\mathrm{sc}}\boldsymbol{F}_{\mathrm{e}}^{-\mathrm{T}}$ is the constitutive part of the solid phase Mandel stress tensor as computed with respect to the natural state, and represents the measure of stress power-conjugate to $\boldsymbol{L}_{\mathrm{p}}$. The prescription on the non-negativeness of D_{rem} is due to the Principle of Maximum Dissipation (cf. e.g. [53]), which is based on the requirement that the overall dissipation function, D_{m}, be non-negative for all possible realisations of the generalised velocities $\phi_{\mathrm{f}}\boldsymbol{v}_{\mathrm{fs}}$ and $\boldsymbol{\ell}_{\mathrm{p}}$ (or $\boldsymbol{L}_{\mathrm{p}}$). Thus, in the case in which the fluid filtration velocity is null, which implies $D_{\mathrm{flow}} = 0$, it must hold that $D_{\mathrm{m}} = D_{\mathrm{rem}} \geq 0$. We remark that the expression of D_{rem} given in (32) appears quite naturally in all the theories of anelastic processes constructed on the BKL decomposition (cf. e.g. [22, 65, 69] for the case of finite strain Elastoplasticity, and [31, 40, 42, 45, 48, 49, 61, 64] for the case of growth and remodelling of biological tissues), and stems from the hypothesis that the strain energy density of the solid phase, $\hat{W}_{\mathrm{s}\kappa}$, can be written as a constitutive function of the elastic part of the overall deformation alone, $\boldsymbol{C}_{\mathrm{e}}$, as done in (9). By relating $\boldsymbol{F}_{\mathrm{p}}$ with the production of material inhomogeneities in uniform bodies [31], a rationale for this constitutive hypothesis is obtained by invoking the Principle of Material Uniformity [29–31, 83].

The second hypothesis is that the solid phase exhibits isotropic elastic behaviour from its natural state. Since this property implies the symmetry of $\boldsymbol{\Sigma}_{\mathrm{sc}\kappa}$, D_{rem} can be rewritten as $D_{\mathrm{rem}} = J_{\mathrm{e}}^{-1}\boldsymbol{\Sigma}_{\mathrm{sc}\kappa} : \boldsymbol{D}_{\mathrm{p}}$. Hence, by exploiting the kinematic identity (4), recalling the relation $J_{\mathrm{p}}\boldsymbol{\Sigma}_{\mathrm{sc}\kappa} = \boldsymbol{\eta}^{-1}\boldsymbol{F}_{\mathrm{p}}^{-\mathrm{T}}\boldsymbol{G}\boldsymbol{\Sigma}_{\mathrm{sc}}\boldsymbol{F}_{\mathrm{p}}^{\mathrm{T}}$ that links $\boldsymbol{\Sigma}_{\mathrm{sc}\kappa}$ with $\boldsymbol{\Sigma}_{\mathrm{sc}}$, and accounting for the symmetry condition (19b), it is possible to show that D_{rem} admits the equivalent form

$$D_{\mathrm{rem}} = -\frac{1}{2J}\left(\boldsymbol{G}\boldsymbol{\Sigma}_{\mathrm{sc}}\boldsymbol{B}_{\mathrm{p}}^{-1}\right) : \dot{\boldsymbol{B}}_{\mathrm{p}}\,. \tag{33}$$

Moreover, since the condition $J_{\mathrm{p}} = 1$ can be rephrased as $\boldsymbol{B}_{\mathrm{p}}^{-1} : \dot{\boldsymbol{B}}_{\mathrm{p}} = 0$, only the deviatoric part of $\boldsymbol{\Sigma}_{\mathrm{sc}}$ contributes to D_{rem}. Consequently, D_{rem} becomes

$$D_{\mathrm{rem}} = -\frac{1}{2J}\left[\boldsymbol{G}\,\mathrm{dev}(\boldsymbol{\Sigma}_{\mathrm{sc}})\boldsymbol{B}_{\mathrm{p}}^{-1}\right] : \dot{\boldsymbol{B}}_{\mathrm{p}} \geq 0\,, \tag{34}$$

with

$$\mathrm{dev}(\boldsymbol{\Sigma}_{\mathrm{sc}}) = \boldsymbol{\Sigma}_{\mathrm{sc}} - \tfrac{1}{3}\mathrm{tr}[\boldsymbol{G}\boldsymbol{\Sigma}_{\mathrm{sc}}]\boldsymbol{G}^{-1}\,. \tag{35}$$

Note that a direct consequence of the hypothesis of isotropy is that the plastic flow rule can be expressed in terms of $\boldsymbol{B}_{\mathrm{p}}$, rather than $\boldsymbol{F}_{\mathrm{p}}$. If, on the one hand, this leads to a loss of information, on the other hand, computations become much lighter.

The third hypothesis concerns the type of remodelling addressed in this paper. As anticipated in Sect. 2.2, we assume that the considered system remodels when the stress induced by external loading exceeds a characteristic threshold, thereby triggering the onset of plastic distortions. Hence, as we would do in the theory of Elastoplasticity, we search for an evolution law for the remodelling variable $\boldsymbol{B}_{\mathrm{p}}$ in the form of a generalised plastic "flow rule". To this end, following [42], we imitate the theory of associative, rate-independent Elastoplasticity [22,93], and articulate in two steps the determination of the flow rule. In the first step, we postulate that a yield surface exists in the space of the deviatoric Kirchhoff stress tensors, which can be defined by the equation

$$f(\boldsymbol{\tau}_{\mathrm{sc}}) := \varphi(\boldsymbol{\tau}_{\mathrm{sc}}) - \sqrt{(2/3)}\,\tau_y = 0\,. \tag{36}$$

Here, $\tau_y > 0$ is a scalar measure of stress playing the role of the "yield stress" of the considered material, and $\varphi(\boldsymbol{\tau}_{\mathrm{sc}})$ is given by

$$\varphi(\boldsymbol{\tau}_{\mathrm{sc}}) := \|\mathrm{dev}(\boldsymbol{\tau}_{\mathrm{sc}})\| = \sqrt{\mathrm{tr}\left[(\boldsymbol{g}\mathrm{dev}(\boldsymbol{\tau}_{\mathrm{sc}}))^2\right]}\,. \tag{37}$$

In the second step, we require that the plastic flow is orthogonal to the yield surface. This leads to the "normality rule" [92,93]

$$\mathcal{L}_{\boldsymbol{v}_{\mathrm{s}}}\boldsymbol{b}_{\mathrm{e}} = -2\gamma_{\mathrm{p}}\boldsymbol{n}\boldsymbol{g}\boldsymbol{b}_{\mathrm{e}}\,, \tag{38}$$

where $\mathcal{L}_{\boldsymbol{v}_{\mathrm{s}}}\boldsymbol{b}_{\mathrm{e}}$ is the Lie derivative of $\boldsymbol{b}_{\mathrm{e}} = \boldsymbol{F}_{\mathrm{e}}\boldsymbol{\eta}^{-1}\boldsymbol{F}_{\mathrm{e}}^{\mathrm{T}} = \boldsymbol{F}\boldsymbol{B}_{\mathrm{p}}\boldsymbol{F}^{\mathrm{T}}$ (i.e., the elastic left Cauchy deformation tensor) with respect to the velocity of the solid phase, $\boldsymbol{v}_{\mathrm{s}}$, $\gamma_{\mathrm{p}} \geq 0$ is a non-negative function of stress, and $\boldsymbol{n}$ is the normalised Kirchhoff stress tensor, orthogonal to the yield surface, defined by

$$\boldsymbol{n}^{\flat} := \boldsymbol{g}\boldsymbol{n}\boldsymbol{g} = \frac{\partial f}{\partial \boldsymbol{\tau}_{\mathrm{sc}}}(\boldsymbol{\tau}_{\mathrm{sc}})\,, \qquad \boldsymbol{n} := \frac{\mathrm{dev}(\boldsymbol{\tau}_{\mathrm{sc}})}{\|\mathrm{dev}(\boldsymbol{\tau}_{\mathrm{sc}})\|}\,. \tag{39}$$

Finally, by exploiting the identity $\mathcal{L}_{\boldsymbol{v}_{\mathrm{s}}}\boldsymbol{b}_{\mathrm{e}} = \boldsymbol{F}\dot{\boldsymbol{B}}_{\mathrm{p}}\boldsymbol{F}^{\mathrm{T}}$, and rewriting (38) as an evolution law for $\boldsymbol{B}_{\mathrm{p}}$, we obtain the equivalent flow rule

$$\dot{\boldsymbol{B}}_{\mathrm{p}} = -2\gamma_{\mathrm{p}}\,\frac{\boldsymbol{B}_{\mathrm{p}}\boldsymbol{G}\mathrm{dev}\,(\boldsymbol{\Sigma}_{\mathrm{sc}})}{\|\mathrm{dev}(\boldsymbol{\tau}_{\mathrm{sc}})\|}\,, \tag{40}$$

where, coherently with [42], we set

$$\gamma_{\mathrm{p}} := \lambda\left[\|\mathrm{dev}(\boldsymbol{\tau}_{\mathrm{sc}})\| - \sqrt{(2/3)}\tau_y\right]_+ = \lambda\,[f(\boldsymbol{\tau}_{\mathrm{sc}})]_+\,. \tag{41}$$

In (38), (40), and (41), γ_{p} is a non-negative "plastic" multiplier, λ is a strictly positive model parameter, and the operator $[\,\cdot\,]_+$ is such that, for any real number A, $[A]_+ = A$, if $A > 0$, and $[A]_+ = 0$ otherwise. The physical units of γ_{p} and λ are $[\gamma_{\mathrm{p}}] = \mathrm{s}^{-1}$ and $[\lambda] = (\mathrm{s}\cdot\mathrm{MPa})^{-1}$, respectively. Equation (40), which represents a stress-driven evolution law for the plastic variable $\boldsymbol{B}_{\mathrm{p}}$, is the remodelling law sought for. We remark that it complies with the prescription $D_{\mathrm{rem}} \geq 0$. Indeed, by substituting (40) into (34), we obtain

$$D_{\mathrm{rem}} = \hat{D}_{\mathrm{rem}}(\boldsymbol{F}, \boldsymbol{B}_{\mathrm{p}}) = \frac{\gamma_{\mathrm{p}}}{J}\|\mathrm{dev}(\boldsymbol{\tau}_{\mathrm{sc}})\| \geq 0\,. \tag{42}$$

If, for a given choice of the model parameters, $\boldsymbol{F}$ and $\boldsymbol{B}_{\mathrm{p}}$ are such that the condition $f(\boldsymbol{\tau}_{\mathrm{sc}}) \leq 0$ applies (which amounts to say that the Frobenius norm of $\boldsymbol{\tau}_{\mathrm{sc}}$ is such that $\|\mathrm{dev}(\boldsymbol{\tau}_{\mathrm{sc}})\| \leq \sqrt{(2/3)}\tau_y$), then it holds that $[f(\boldsymbol{\tau}_{\mathrm{sc}})]_+ = 0$ and, consequently, the plastic multiplier γ_{p} vanishes identically, thereby implying that $D_{\mathrm{rem}} = 0$. In this situation, no remodelling occurs, and the material deforms while preserving its internal structure. However, when $\|\mathrm{dev}(\boldsymbol{\tau}_{\mathrm{sc}})\|$ exceeds the threshold stress $\sqrt{(2/3)}\tau_y$ (i.e., when $f(\boldsymbol{\tau}_{\mathrm{sc}}) > 0$), remodelling takes place, and $\boldsymbol{B}_{\mathrm{p}}$ evolves as prescribed by (40). In this case, D_{rem} becomes

$$D_{\mathrm{rem}} = \frac{\lambda[f(\boldsymbol{\tau}_{\mathrm{sc}})]_+}{J}\|\mathrm{dev}(\boldsymbol{\tau}_{\mathrm{sc}})\| > 0\,. \tag{43}$$

A relevant difference between the model presented so far and the standard model of associative, rate-independent J_2-plasticity is that γ_{p} does not stem from any optimality condition of the Karush-Kuhn-Tucker type [22, 93]. Rather, γ_{p} is defined phenomenologically, and, in the biological context analysed in [42], it expresses the fact that a cellular aggregate, in which the stress exceeds a prescribed threshold value, reorganises its internal structure by breaking the adhesion bonds connecting the cells. Note also that no hardening is considered in this biological problem.

3.2 Summary of the mathematical model

The mathematical model presented in this paper is grounded on the mass balance law (28), the balance law of linear momentum (14), and on the flow rule (40). Thus, in summary, we have to solve the following set of equations:

$$\dot{J} - \mathrm{Div}\left[\hat{\boldsymbol{K}}(\boldsymbol{F})\mathrm{Grad}\,p\right] = 0\,, \tag{44a}$$

$$\mathrm{Div}\left(-Jp\,\boldsymbol{g}^{-1}\boldsymbol{F}^{-\mathrm{T}} + \hat{\boldsymbol{P}}_{\mathrm{sc}}(\boldsymbol{F}, \boldsymbol{B}_{\mathrm{p}})\right) = \boldsymbol{0}\,, \tag{44b}$$

$$\dot{\boldsymbol{B}}_{\mathrm{p}} + \hat{\mathfrak{R}}(\boldsymbol{F}, \boldsymbol{B}_{\mathrm{p}}) = \boldsymbol{0}\,, \tag{44c}$$

in which $\hat{\boldsymbol{K}}(\boldsymbol{F})$ and $\hat{\boldsymbol{P}}_{\mathrm{sc}}(\boldsymbol{F}, \boldsymbol{B}_{\mathrm{p}})$ are defined in (29b) and (15), respectively, $\hat{\mathfrak{R}}(\boldsymbol{F}, \boldsymbol{B}_{\mathrm{p}})$ stands for

$$\mathfrak{R} \equiv \hat{\mathfrak{R}}(\boldsymbol{F}, \boldsymbol{B}_{\mathrm{p}}) := 2\gamma_{\mathrm{p}}\,\frac{\boldsymbol{B}_{\mathrm{p}}\boldsymbol{G}\mathrm{dev}(\boldsymbol{\Sigma}_{\mathrm{sc}})}{\|\mathrm{dev}(\boldsymbol{\tau}_{\mathrm{sc}})\|}\,, \tag{45}$$

and γ_{p} is specified in (41). The model equations (44a)–(44c) are equivalent to a set of ten scalar equations in the ten unknowns represented by the three components of the solid phase motion, χ, pressure, p, and the six independent components of the symmetric second-order tensor $\boldsymbol{B}_{\mathrm{p}}$. The model is thus closed. Moreover, it is completed by the following boundary conditions:

$$\chi = \chi_{\mathrm{b}}, \qquad \text{on } \varGamma_{\mathrm{D}}^{\chi}, \tag{46a}$$

$$\left(-Jp\,\boldsymbol{g}^{-1}\boldsymbol{F}^{-\mathrm{T}} + \hat{\boldsymbol{P}}_{\mathrm{sc}}(\boldsymbol{F},\boldsymbol{B}_{\mathrm{p}})\right).\boldsymbol{N} = \boldsymbol{f}_{\mathrm{R}}, \qquad \text{on } \varGamma_{\mathrm{N}}^{\chi}, \tag{46b}$$

$$p = p_{\mathrm{b}}, \qquad \text{on } \varGamma_{\mathrm{D}}^{p}, \tag{46c}$$

$$\left(-\hat{\boldsymbol{K}}(\boldsymbol{F})\mathrm{Grad}\,p\right).\boldsymbol{N} = Q_{\mathrm{b}}, \qquad \text{on } \varGamma_{\mathrm{N}}^{p}. \tag{46d}$$

In (46), $\boldsymbol{N}$ is the unit vector normal to $\partial\mathcal{C}_{\mathrm{R}}$, i.e., the boundary of the reference configuration $\mathcal{C}_{\mathrm{R}}$, and the sets $\varGamma_{\mathrm{D}}^{\chi}$ and $\varGamma_{\mathrm{D}}^{p}$ are the Dirichlet-portions of $\partial\mathcal{C}_{\mathrm{R}}$, on which the deformation, χ, and the pressure, p, are equal to the prescribed data χ_{b} and p_{b}, respectively. Analogously, $\varGamma_{\mathrm{N}}^{\chi}$ and $\varGamma_{\mathrm{N}}^{p}$ are the Neumann-portions of $\partial\mathcal{C}_{\mathrm{R}}$, on which the contact force, $\boldsymbol{f}_{\mathrm{R}}$, and the fluid flux, Q_{b}, are supplied, respectively. It holds that $\partial\mathcal{C}_{\mathrm{R}} = \varGamma_{\mathrm{D}}^{\chi} \sqcup \varGamma_{\mathrm{N}}^{\chi} = \varGamma_{\mathrm{D}}^{p} \sqcup \varGamma_{\mathrm{N}}^{p}$. The values assigned to χ_{b}, p_{b}, $\boldsymbol{f}_{\mathrm{R}}$, and Q_{b} are problem-dependent and should be discussed on a case-by-case basis. In the following, however, we shall restrict our formulation to a problem obeying Neumann-zero boundary conditions on $\varGamma_{\mathrm{N}}^{\chi}$ and $\varGamma_{\mathrm{N}}^{p}$, which implies $Q_{\mathrm{b}} = 0$ and $\boldsymbol{f}_{\mathrm{R}} = \boldsymbol{0}$. Finally, initial conditions are needed because (44a) and (44c) feature the time derivatives of the volumetric ratio, J, and of the anelastic deformation tensor $\boldsymbol{B}_{\mathrm{p}}$, respectively. Here, we assume the following initial conditions:

$$J(X,t_0) = 1, \qquad \forall\, X \in \mathcal{C}_{\mathrm{R}}, \tag{47a}$$

$$\boldsymbol{B}_{\mathrm{p}}(X,t_0) = \boldsymbol{G}^{-1}, \qquad \forall\, X \in \mathcal{C}_{\mathrm{R}}. \tag{47b}$$

For the sake of simplicity, we assume now that the tissue is homogeneous. Thus, all the elements of the sets of parameters $\{\alpha_0,\alpha_1,\alpha_2,\beta\}$ and $\{m_0,m_1\}$, which characterise, respectively, the strain energy density function, $\hat{W}_{\mathrm{s}\kappa}$, and the hydraulic conductivity, $\boldsymbol{k}$, are regarded as constants. We assume that also ϕ_{sR} and $k_{0\mathrm{R}}$ are constants. Clearly, the hypotheses of homogeneity and isotropy provide a poor approximation of real tissues. Nonetheless, they are useful hypotheses at this stage, since they help to better visualise the influence of remodelling on the mechanical and fluid dynamic properties of the specimen.

4 Numerics

The numerical procedure elaborated in this paper to solve (44a)–(44c) is based on the Finite Element Method. Therefore, it is necessary to start with the weak formulation of (44a) and (44b). Although there exist numerical strategies that perform finite element discretisations also for the plastic flow rule [32], we prefer here to keep (44c) in local form. This is legitimate since it involves no partial derivative with respect to space coordinates. Before proceeding, we notice that the particular choice of the constitutive law expressing the hydraulic conductivity, $\boldsymbol{K} = \hat{\boldsymbol{K}}(\boldsymbol{F})$, is such that the mass balance law (44a) does not contain $\boldsymbol{B}_{\mathrm{p}}$. This weakens the coupling among the model equations, as will be discussed in Sect. 6. Our procedure, however, can be generalised to the cases in which constitutive laws of the type $\boldsymbol{K} = \hat{\boldsymbol{K}}(\boldsymbol{F}, \boldsymbol{B}_{\mathrm{p}})$ are employed.

4.1 Weak Formulation

The weak form of (44a) and (44b) is given by

$$\mathfrak{F}_p(p, \chi, \tilde{p}) := -\int_{\mathcal{C}_{\mathrm{R}}} \left\{(\mathrm{Grad}\,\tilde{p})\left[\hat{\boldsymbol{K}}(\boldsymbol{F})\mathrm{Grad}\,p\right] + \tilde{p}\,\dot{J}\right\} = 0\,, \tag{48a}$$

$$\mathfrak{F}_\chi(p, \chi, \boldsymbol{B}_{\mathrm{p}}, \tilde{\boldsymbol{u}}) := \int_{\mathcal{C}_{\mathrm{R}}} \hat{\boldsymbol{P}}(p, \boldsymbol{F}, \boldsymbol{B}_{\mathrm{p}}) : \boldsymbol{g}\mathrm{Grad}\,\tilde{\boldsymbol{u}} = 0\,, \tag{48b}$$

where $\hat{\boldsymbol{P}}(p, \boldsymbol{F}, \boldsymbol{B}_{\mathrm{p}})$ is defined in (16), and we introduced the space of test functions

$$\tilde{\mathcal{P}} \times \tilde{\boldsymbol{\mathcal{V}}} := \{(\tilde{p}, \tilde{\boldsymbol{u}}) \in H^1_0(\mathcal{C}_{\mathrm{R}}) \times \mathbf{H}^1_0(\mathcal{C}_{\mathrm{R}}) \,:\, \tilde{p}\big|_{\Gamma^p_{\mathrm{D}}} = 0\,,\ \tilde{\boldsymbol{u}}\big|_{\Gamma^\chi_{\mathrm{D}}} = \mathbf{0}\}\,. \tag{49}$$

In (48) and (49), $\tilde{p}$ and $\tilde{\boldsymbol{u}}$ denote the test pressure and the test velocity. As such, both fields satisfy homogeneous Dirichlet boundary conditions. The functional spaces $H^1_0(\mathcal{C}_{\mathrm{R}})$ and $\mathbf{H}^1_0(\mathcal{C}_{\mathrm{R}})$ are, respectively, the Sobolev spaces of all scalar-valued and vector-valued functions vanishing on Γ^p_{D} and Γ^χ_{D}, square-integrable in $\mathcal{C}_{\mathrm{R}}$, and whose weak derivatives of order $m \leq 1$ are all square-integrable in $\mathcal{C}_{\mathrm{R}}$ too. We recall that (48a) and (48b) are obtained by multiplying (44a) by $\tilde{p}$ and (44b) by $\tilde{\boldsymbol{u}}$, and applying Gauss' Theorem [59]. By construction, the functionals $\mathfrak{F}_p$ and $\mathfrak{F}_\chi$ are linear in $\tilde{p}$ and $\tilde{\boldsymbol{u}}$, respectively. For the sake of a lighter notation, we omit the explicit dependence of $\mathfrak{F}_p$ and $\mathfrak{F}_\chi$ on the test fields $\tilde{p}$ and $\tilde{\boldsymbol{u}}$ in the forthcoming discussion. This dependence is, however, understood. Finally, we notice that the use of Darcy's law to describe the fluid flow implies that both $\mathfrak{F}_p$ and $\mathfrak{F}_\chi$ are affine with respect to the pressure p.

4.2 Time-discrete setting

The time-discrete version of (48a), (48b) and (44c) is obtained by performing an implicit Euler finite difference scheme. To this end, we discretise the time interval $\mathcal{I}$, over which the system is observed, into N disjoint subintervals $[t_{n-1}, t_n]$, with $n \geq 1$, $n \in \mathbb{N}$, and replace the derivatives $\dot{J}$ and $\dot{\boldsymbol{B}}_{\mathrm{p}}$ with the expressions $(J_n - J_{n-1})/\Delta t_n$ and $(\boldsymbol{B}_{\mathrm{p}n} - \boldsymbol{B}_{\mathrm{p}(n-1)})/\Delta t_n$, where Δt_n is the size of the nth time-step. From here on, given an arbitrary function f of space and time, the notation $f_n(X)$, or simply f_n, stands for $f(X, t_n)$, for all values of n.

The initial instant of time t_0 corresponds to the reference, undeformed configuration, $\mathcal{C}_{\mathrm{R}}$, in which $J_0 = J(X, t_0) = 1$. We also set $\boldsymbol{B}_{\mathrm{p}0} = \boldsymbol{B}_{\mathrm{p}}(X, t_0) = \boldsymbol{G}^{-1}$, thereby implying that no plastic distortion is associated with the initial state of the solid phase. At the nth instant of time, $n \geq 1$, the time-discrete model equations become:

$$\mathfrak{F}_p(p_n, \chi_n) := -\int_{\mathcal{C}_\mathrm{R}} \left\{ (\mathrm{Grad}\, \tilde{p})\, [\boldsymbol{K}_n \mathrm{Grad}\, p_n] + \tilde{p}\, \frac{J_n - J_{n-1}}{\Delta t_n} \right\} = 0\,, \quad \text{(50a)}$$

$$\mathfrak{F}_\chi(p_n, \chi_n, \boldsymbol{B}_{\mathrm{p}n}) := \int_{\mathcal{C}_\mathrm{R}} \hat{\boldsymbol{P}}(p_n, \boldsymbol{F}_n, \boldsymbol{B}_{\mathrm{p}n}) : \boldsymbol{g}\mathrm{Grad}\, \tilde{\boldsymbol{u}} = 0\,, \quad \text{(50b)}$$

$$\mathcal{G}(\chi_n, \boldsymbol{B}_{\mathrm{p}n}) := \boldsymbol{B}_{\mathrm{p}n} - \boldsymbol{B}_{\mathrm{p}(n-1)} + \Delta t_n \hat{\boldsymbol{\mathfrak{R}}}(\boldsymbol{F}_n, \boldsymbol{B}_{\mathrm{p}n}) = \boldsymbol{0}\,. \quad \text{(50c)}$$

The notation $\mathcal{G}(\chi_n, \boldsymbol{B}_{\mathrm{p}n})$ means that the time-discrete form of the plastic flow rule is a function of $\boldsymbol{B}_{\mathrm{p}n}$, and a "functional" of the deformation, χ_n, through the deformation gradient tensor, $\boldsymbol{F}_n$ [19]. Equations (50a)–(50c) are now solved sequentially for varying $n \geq 1$. Apart from (50c), the formulation of (50a) and (50b) largely follows the procedure presented in [44].

4.3 Linearisation and Finite Element Discretisation

In this section, we demonstrate in detail the computational procedure, adapted from [47], that is used to solve numerically (50a)–(50c). We search for solutions to the problem (50a)–(50c) by means of a linearisation algorithm based on the Newton method, and articulated in two stages. In addition to n, we introduce two other subscripts: For each n, $l \in \mathbb{N}$ and $k \in \mathbb{N}$ count the iterations with respect to $\boldsymbol{B}_{\mathrm{p}n}$ and the pair (p_n, χ_n), respectively. Consequently, we construct the sequences

$$\chi_{n,k} = \chi_{n,k-1} + \boldsymbol{h}_{n,k}, \quad \text{(51a)}$$

$$p_{n,k} = p_{n,k-1} + \pi_{n,k}, \quad \text{(51b)}$$

$$\boldsymbol{B}_{\mathrm{p}n,l} = \boldsymbol{B}_{\mathrm{p}n,l-1} + \boldsymbol{\Phi}_{\mathrm{p}n,l}\,, \qquad k, l \geq 1 \quad \text{(51c)}$$

with $\boldsymbol{h}_{n,k}$, $\pi_{n,k}$, and $\boldsymbol{\Phi}_{\mathrm{p}n,l}$ being the increments associated with χ_n, p_n, and $\boldsymbol{B}_{\mathrm{p}n}$, respectively. Moreover, for conciseness, we adopt the notation

$$w_n := (p_n, \chi_n)\,, \quad \text{(52a)}$$

$$\Theta_{n,l-1} := (\chi_n, \boldsymbol{B}_{\mathrm{p}n,l-1})\,, \quad \text{(52b)}$$

$$\Lambda_{n,l-1} := (p_n, \chi_n, \boldsymbol{B}_{\mathrm{p}n,l-1})\,. \quad \text{(52c)}$$

In the first stage of the algorithm, we linearise (50b) and (50c) with respect to $\boldsymbol{B}_{\mathrm{p}n}$ only. The linearisation is done in a neighbourhood of $\Lambda_{n,l-1}$ and $\Theta_{n,l-1}$, respectively, and leads to the approximated expressions

$$\mathfrak{F}^{(1)}_\chi(\Lambda_{n,l-1}, \boldsymbol{\Phi}_{n,l}) := \mathfrak{F}_\chi(\Lambda_{n,l-1}) + D_{\boldsymbol{B}_\mathrm{p}} \mathfrak{F}_\chi(\Lambda_{n,l-1})[\boldsymbol{\Phi}_{n,l}]\,, \quad \text{(53a)}$$

$$\mathcal{G}^{(1)}(\Theta_{n,l-1}, \boldsymbol{\Phi}_{n,l}) := \mathcal{G}(\Theta_{n,l-1}) + \mathbb{Y}(\Theta_{n,l-1}) : \boldsymbol{\Phi}_{n,l}\,, \quad \text{(53b)}$$

where $D_{\boldsymbol{B}_{\rm p}}\mathfrak{F}_\chi(\Lambda_{n,l-1})[\boldsymbol{\Phi}_{n,l}]$ denotes the Gâteaux derivative of $\mathfrak{F}_\chi$, computed at $\Lambda_{n,l-1}$ along the direction of the plastic increment $\boldsymbol{\Phi}_{n,l}$ [19,93], and $\mathbb{Y}(\Theta_{n,l-1})$ is the fourth-order tensor defined by

$$\mathbb{Y}(\Theta_{n,l-1}) = \frac{\partial \mathfrak{G}}{\partial \boldsymbol{B}_{{\rm p}n}}(\Theta_{n,l-1}) \in [T\mathcal{C}_{\rm R}]^2{}_2 \,. \tag{54}$$

Note that $\mathbb{Y}(\Theta_{n,l-1})$ is pair-symmetric, i.e., in its component representation, it holds that

$$[\mathbb{Y}(\Theta_{n,l-1})]^{AB}{}_{CD} = [\mathbb{Y}(\Theta_{n,l-1})]^{BA}{}_{CD} \,, \tag{55a}$$

$$[\mathbb{Y}(\Theta_{n,l-1})]^{AB}{}_{CD} = [\mathbb{Y}(\Theta_{n,l-1})]^{AB}{}_{DC} \,. \tag{55b}$$

We remark that also $\mathfrak{F}_p$ has to be linearised in the same fashion as $\mathfrak{F}_\chi$ in the cases in which it involves $\boldsymbol{B}_{{\rm p}n}$ among its arguments (e.g., if the hydraulic conductivity depends on $\boldsymbol{B}_{\rm p}$).

We now set $\mathfrak{G}^{(1)}(\Theta_{n,l-1}, \boldsymbol{\Phi}_{n,l}) = \boldsymbol{0}$, and solve for $\boldsymbol{\Phi}_{n,l}$, thereby obtaining

$$\boldsymbol{\Phi}_{n,l} \equiv \hat{\boldsymbol{\Phi}}(\Theta_{n,l-1}) = -[\mathbb{Y}(\Theta_{n,l-1})]^{-1} : \mathfrak{G}(\Theta_{n,l-1}) \,. \tag{56}$$

In this way, the increment $\boldsymbol{\Phi}_{n,l}$ is written as a function of χ_n. This allows to eliminate statically $\boldsymbol{\Phi}_{n,l}$ from $\mathfrak{F}_\chi^{(1)}$. Indeed, by substituting the right-hand-side of (56) into (53a), we obtain the new functional

$$\mathfrak{F}_\chi^{(2)}(\Lambda_{n,l-1}) = \mathfrak{F}_\chi(\Lambda_{n,l-1}) - \mathfrak{L}(\Lambda_{n,l-1}) \,, \tag{57}$$

where the auxiliary quantity $\mathfrak{L}(\Lambda_{n,l-1})$ reads

$$\mathfrak{L}(\Lambda_{n,l-1}) := D_{\boldsymbol{B}_{\rm p}}\mathfrak{F}_\chi(\Lambda_{n,l-1}) \left[[\mathbb{Y}(\Theta_{n,l-1})]^{-1} : \mathfrak{G}(\Theta_{n,l-1}) \right] \,. \tag{58}$$

In (56), the inversion of $\mathbb{Y}$ is performed as follows. Let d denote the dimension of the tangent space $T_X\mathcal{C}_{\rm R}$ at $X \in \mathcal{C}_{\rm R}$ (e.g., $d = \dim(T_X\mathcal{C}_{\rm R}) = 3$). Since $\mathbb{Y}$ is a fourth-order tensor, it has d^4 components in the representation

$$\mathbb{Y} = Y^{AB}{}_{CD} \boldsymbol{E}_A \otimes \boldsymbol{E}_B \otimes \boldsymbol{E}^C \otimes \boldsymbol{E}^D \,,$$

where $\{\boldsymbol{E}_M\}_{M=1}^d \subset T_X\mathcal{C}_{\rm R}$ and $\{\boldsymbol{E}^M\}_{M=1}^d \subset T_X^*\mathcal{C}_{\rm R}$ are bases of $T_X\mathcal{C}_{\rm R}$ and $T_X^*\mathcal{C}_{\rm R}$, respectively. Now, the set of d^4 scalars $[Y^{AB}{}_{CD}]$ is identified with a $d^2 \times d^2$ matrix $[\mathsf{Y}]$, which can be inverted by means of standard methods. In this work, we used a LU-decomposition. We remark that, due to the spatial discretisation of the Finite Element Method, this LU-decomposition needs to be performed at every integration point of an element. The inverse matrix $[\mathsf{Y}^{-1}]$ is thus a representation of the fourth-order tensor $\mathbb{Y}^{-1}$. Note that, in (56), the second-order tensor $\mathfrak{G}$ is represented as a vector-like column array G with d^2 entries.

Now, for fixed $\boldsymbol{B}_{{\rm p}n,l-1}$, with $l \geq 1$, we determine pressure and deformation by solving iteratively the sub-problem

$$\mathfrak{F}_\chi^{(2)}(\Lambda_{n,l-1}) = 0 \,, \tag{59a}$$

$$\mathfrak{F}_p(w_n) = 0 \,. \tag{59b}$$

At the kth iteration, $k \geq 1$, we define

$$w_{n,k} := (p_{n,k}, \chi_{n,k}) \,, \tag{60a}$$
$$\Theta_{n,k,l-1} := (\chi_{n,k}, \boldsymbol{B}_{\mathrm{p}n,l-1}) \,, \tag{60b}$$
$$\Lambda_{n,k,l-1} := (p_{n,k}, \chi_{n,k}, \boldsymbol{B}_{\mathrm{p}n,l-1}) \,, \tag{60c}$$

and apply a Newton method to (59a) and (59b). That is, we solve the linearised set of equations

$$a(\boldsymbol{h}_{n,k}, \tilde{\boldsymbol{u}}) - b(\tilde{\boldsymbol{u}}, \pi_{n,k}) = -\mathfrak{F}_{\chi}^{(2)}(\Lambda_{n,k-1,l-1}) \,, \tag{61a}$$
$$-c(\boldsymbol{h}_{n,k}, \tilde{p}) - d(\pi_{n,k}, \tilde{p}) = -\mathfrak{F}_p(w_{n,k-1}) \,. \tag{61b}$$

In (61a) and (61b), the bilinear forms $a(\,\cdot\,,\,\cdot\,)$, $b(\,\cdot\,,\,\cdot\,)$, $c(\,\cdot\,,\,\cdot\,)$ and $d(\,\cdot\,,\,\cdot\,)$ are defined by means of the Gâteaux derivatives of the functionals $\mathfrak{F}_{\chi}^{(2)}$ and $\mathfrak{F}_p$:

$$\begin{aligned}
a(\boldsymbol{h}_{n,k}, \tilde{\boldsymbol{u}}) =& D_{\chi}\mathfrak{F}_{\chi}^{(2)}(\Lambda_{n,k-1,l-1})[\boldsymbol{h}_{n,k}] && \text{(62a)}\\
=& \int_{\mathcal{C}_{\mathrm{R}}} \boldsymbol{g}\mathrm{Grad}\,\tilde{\boldsymbol{u}} : \mathbb{A}^{(2)}_{n,k-1,l-1} : \boldsymbol{H}_{n,k} \,, \\
-b(\tilde{\boldsymbol{u}}, \pi_{n,k}) =& D_p\mathfrak{F}_{\chi}^{(2)}(\Lambda_{n,k-1,l-1})[\pi_{n,k}] && \text{(62b)}\\
=& \int_{\mathcal{C}_{\mathrm{R}}} \left\{ -J_{n,k-1}\pi_{n,k}\, \boldsymbol{F}^{-\mathrm{T}}_{n,k-1} : \mathrm{Grad}\,\tilde{\boldsymbol{u}} \right\} \,, \\
-c(\boldsymbol{h}_{n,k}, \tilde{p}) =& D_{\chi}\mathfrak{F}_p(w_{n,k-1})[\boldsymbol{h}_{n,k}] && \text{(62c)}\\
=& -\int_{\mathcal{C}_{\mathrm{R}}} \{(\mathrm{Grad}\,\tilde{p})\,[(\mathbb{K}_{n,k-1} : \boldsymbol{H}_{n,k})\,\mathrm{Grad}\,p_{n,k-1}]\} \\
& - \frac{b(\boldsymbol{h}_{n,k}, \tilde{p})}{\Delta t_n} \,, \\
-d(\pi_{n,k}, \tilde{p}) =& D_p\mathfrak{F}_p(w_{n,k-1})[\pi_{n,k}] && \text{(62d)}\\
=& -\int_{\mathcal{C}_{\mathrm{R}}} (\mathrm{Grad}\,\tilde{p})\,[\boldsymbol{K}_{n,k-1}\mathrm{Grad}\,\pi_{n,k}] \,,
\end{aligned}$$

where $\boldsymbol{H}_{n,k} = \mathrm{Grad}\,\boldsymbol{h}_{n,k}$, and the tensors $\mathbb{A}^{(2)}_{n,k-1,l-1}$, $\mathbb{K}_{n,k-1}$ and $\boldsymbol{K}_{n,k-1}$ are given by

$$\begin{aligned}
\mathbb{A}^{(2)}_{n,k-1,l-1} =& -J_{n,k-1}p_{n,k-1}\boldsymbol{g}^{-1}\boldsymbol{F}^{-\mathrm{T}}_{n,k-1} \otimes \boldsymbol{F}^{-\mathrm{T}}_{n,k-1} && \text{(63a)}\\
& + J_{n,k-1}p_{n,k-1}\boldsymbol{g}^{-1}\boldsymbol{F}^{-\mathrm{T}}_{n,k-1} \,\overline{\otimes}\, \boldsymbol{F}^{-1}_{n,k-1} \\
& + \left(\mathbb{A}^{\mathrm{sc}}_{n,k-1,l-1} - \mathbb{L}_{n,k-1,l-1}\right) \,,
\end{aligned}$$

$$\mathbb{K}_{n,k-1} = \frac{\partial \hat{\boldsymbol{K}}}{\partial \boldsymbol{F}}(\boldsymbol{F}_{n,k-1}) \,, \tag{63b}$$
$$\boldsymbol{K}_{n,k-1} = \hat{\boldsymbol{K}}(\boldsymbol{F}_{n,k-1}) \,. \tag{63c}$$

In particular, $\mathbb{A}^{\mathrm{sc}}_{n,k-1,l-1}$ is the constitutive acoustic tensor computed at the lth iteration in $\boldsymbol{B}_{\mathrm{p}n}$ and at the kth iteration in χ_n, i.e.,

$$\mathbb{A}^{\mathrm{sc}}_{n,k-1,l-1} = \frac{\partial \hat{\boldsymbol{P}}_{\mathrm{sc}}}{\partial \boldsymbol{F}}(\boldsymbol{F}_{n,k-1}, \boldsymbol{B}_{\mathrm{p}n,l-1}) \,, \tag{64}$$

while $\mathbb{L}_{n,k-1,l-1}$ is a fictitious acoustic tensor, introduced by the algorithm, and induced by the Gâteaux derivative of the functional $\mathfrak{L}$ with respect to the deformation (cf. (58)), i.e.,

$$D_{\chi}\mathfrak{L}(\Lambda_{n,k-1,l-1})[\boldsymbol{h}_{n,k}] := \int_{\mathcal{C}_{\mathrm{R}}} \boldsymbol{g}\mathrm{Grad}\,\tilde{\boldsymbol{u}} : \mathbb{L}_{n,k-1,l-1} : \boldsymbol{H}_{n,k}\,. \tag{65}$$

It is important to remark that the effective acoustic tensor

$$\left(\mathbb{A}^{\mathrm{sc}}_{n,k-1,l-1} - \mathbb{L}_{n,k-1,l-1}\right)$$

should be positive definite (cf., for example, [17,18]). Although our numerical simulations produced reasonable results, we have not formulated theorems yet, which predict when this condition fails to be satisfied.

The algorithm proposed in this paper requires a linearisation with respect to χ_n and one with respect to $\boldsymbol{B}_{\mathrm{p}n}$. Therefore, compared with the classical RMA [93], an additional linearisation iteration is performed. This increases the computational effort, but makes our algorithm more flexible and suitable for various types of remodelling laws, which could also be much more complicated than the one given in (41).

The numerical method presented in this work has been implemented in UG4, a novel version of the software framework UG ("Unstructured Grids")[96]. Its algebra, discretisation and grid libraries as well as its massive-parallel solvers for coupled partial differential equations served as a basis for computing a benchmark problem of the presented poroplastic model.

5 Results

The unconfined compression test is a very common experimental procedure that is performed to determine the mechanical and fluid dynamic properties of hydrated soft tissues, such as articular cartilage [51]. In this benchmark, a sample of tissue is inserted between two rigid and impermeable parallel plates, and compressed according to some prescribed loading protocol, which can be either in force- or in displacement-control. During compression, the parts of the specimen's boundary that are not in contact with the plates, and through which the interstitial fluid can escape, can expand freely.

For our simulations, we consider a cylindrical specimen of biphasic material characterised by initial height $H_0 = 1$ mm and initial radius $R_0 = 1.5$ mm. The lower boundary of the specimen is clamped at the lower plate of the experimental apparatus and kept fixed. The upper boundary, instead, is in contact with the moving plate and is assumed to expand without friction in axial-symmetric way. Finally, the lateral boundary of the specimen is traction-free and permeable to fluid flow. The above description of the experiment can be translated into mathematical formulae as follows: let Γ_{l}, Γ_{L}, and Γ_{u} be the lower, lateral, and upper boundaries of the specimen in its undeformed configuration (which is taken coincident with the reference configuration), i.e., $\partial\mathcal{C}_{\mathrm{R}} = \Gamma_{\mathrm{l}} \cup \Gamma_{\mathrm{L}} \cup \Gamma_{\mathrm{u}}$. Then, for all $t \in \mathcal{I} \equiv [0, T]$, we prescribe:

$$\text{on } \Gamma_{\mathrm{l}}, \quad \begin{cases} \chi(X,t) = \chi(X,0) = X \in \Gamma_{\mathrm{l}}, \\ (-\boldsymbol{K}\,\mathrm{Grad}\,p)\,.\boldsymbol{N} = 0, \end{cases} \tag{66a}$$

$$\text{on } \Gamma_{\mathrm{L}}, \quad \begin{cases} \left(-Jp\,\boldsymbol{g}^{-1}\boldsymbol{F}^{-\mathrm{T}} + \boldsymbol{P}_{\mathrm{sc}}\right).\boldsymbol{N} = \boldsymbol{0}, \\ p = 0, \end{cases} \tag{66b}$$

$$\text{on } \Gamma_{\mathrm{u}}, \quad \begin{cases} \chi^z(X,t) = \chi^z_{\mathrm{b}}(t)\,[\Theta(t) - \Theta(t-T_0)] + \chi^z_{\mathrm{b}}(T_0)\Theta(t-T_0), \\ (-\boldsymbol{K}\,\mathrm{Grad}\,p)\,.\boldsymbol{N} = 0, \end{cases} \tag{66c}$$

where Θ is the Heaviside function (here defined such that $\Theta(\xi) = 1$, if $\xi \geq 0$, and $\Theta(\xi) = 0$, if $\xi < 0$), χ^z_{b} is the axial compressive deformation imposed at the upper boundary, i.e.,

$$\chi^z_{\mathrm{b}}(t) = H_0/2 - u_{\mathrm{T}}\frac{t}{T_0}\,, \tag{67}$$

$T_0 \in (0, T)$ is the final instant of time of the loading ramp, and $u_{\mathrm{T}} > 0$ is the target displacement (here, we took $u_{\mathrm{T}} = 0.15$ mm). To observe how the perturbed system relaxes towards a stationary state, we took $T_0 = 30$ s and $T = 80$ s. Looking at (66a)–(66c), it is clear that the Dirichlet- and Neumann-like subsets of $\partial\mathcal{C}_{\mathrm{R}}$ associated with the deformation, $\Gamma^{\chi}_{\mathrm{D}}$ and $\Gamma^{\chi}_{\mathrm{N}}$, are given by $\Gamma^{\chi}_{\mathrm{D}} = \Gamma_{\mathrm{l}} \cup \Gamma_{\mathrm{u}}$ and $\Gamma^{\chi}_{\mathrm{N}} = \Gamma_{\mathrm{L}}$, respectively, while it holds that $\Gamma^{p}_{\mathrm{D}} = \Gamma_{\mathrm{L}}$ and $\Gamma^{p}_{\mathrm{N}} = \Gamma_{\mathrm{l}} \cup \Gamma_{\mathrm{u}}$ for the pressure.

The material parameters used for this test are reported in Table 1. The elastic coefficients for the Holmes-Mow strain energy density given in (10a) are selected in such a way that $\beta = \alpha_1 + 2\alpha_2 = 1$ [57].

Table 1 material parameters

elastic coefficient	α_0	$0.125\,\mathrm{N/mm^2}$
elastic coefficient	α_1	0.78
elastic coefficient	α_2	0.11
elastic coefficient	β	1.0
referential hydraulic conductivity	$k_{0\mathrm{R}}$	$3.7729 \cdot 10^{-3}\,\mathrm{mm^4/(N \cdot s)}$
material parameter	m_0	0.0848
material parameter	m_1	4.638
referential solidity	ϕ_{sR}	0.2
initial yields stress	τ_y	$0.002\,\mathrm{N/mm^2}$
coefficient in the plastic flow rule	λ	$0.5\,\mathrm{mm^2/(N \cdot s)}$

The results of our numerical tests, reported in Figs. 3-5, are plotted on a section of the specimen containing the symmetry axis.

To highlight the influence of the plastic distortions on the mechanical and fluid dynamic response of the specimen, we compared the radial and axial components of the fluid filtration velocity, the pressure distribution, and the first invariant of the constitutive part of the Mandel stress tensor obtained in the poroelastic case (left column of Fig. 3) with those obtained in the presence of plastic distortions, i.e., in the poroplastic case (right column of Fig. 3). To characterise the poroelastic case, we simulated an unconfined compression test in which the yields stress, τ_y, which determines the onset of plastic flow, was set equal to a value that is never reached by the stress in the tissue. More precisely, we chose $\tau_y = 2000.00\,\mathrm{N/mm}^2$, a value that led to a purely elastic material response. In this situation, it holds that $\boldsymbol{B}_\mathrm{p} = \boldsymbol{G}^{-1}$ at all times of the observation time interval. In the poroplastic case, instead, $\boldsymbol{B}_\mathrm{p}$ is determined by means of the numerical procedure reported in Sect. 4. Figures 5(a) and 5(b) show the first and second invariant of $\boldsymbol{B}_\mathrm{p}$ at the end of the loading ramp, i.e., at $t = 30$ s. We found that the higher values of these invariants are attained at the points of the specimen's boundary corresponding to the intersection of Γ_l and Γ_L.

Before commenting our results, we recall that, in this paper, remodelling is entirely described in terms of "plastic" distortions. Thus, plotting figures in which plastic distortions are switched off actually means to show the results in which no remodelling occurs.

Looking at Fig. 3, we notice that the influence of remodelling manifests itself through the modulation of the fluid filtration velocity, the change of the pore pressure distribution, and the lowering of the constitutive part of the stress of the solid phase. In particular, Figs. 3(a) and 3(b) show that the magnitudes of the radial and the axial filtration velocity, computed according to Darcy's law, i.e., $\phi_\mathrm{f} \boldsymbol{v}_\mathrm{fs} = -\boldsymbol{k} \,\mathrm{grad}\, p$, decrease in the poroplastic case. In Figs. 3(a) and 3(b), the arrows represent the local direction of the flow. The decrease of the magnitude of the filtration velocity characterising the poroplastic case is related to the decrease of the pore pressure (see Fig. 3(c)) and the decrease of stress, which in Fig. 3(d) is accounted for by the first invariant of $\boldsymbol{\Sigma}_\mathrm{sc}$. The values of the first invariant of $\boldsymbol{\Sigma}_\mathrm{sc}$ are computed with respect to the reference configuration. However, in a visualisation post-process, the reference configuration is deformed by the motion map, so that the previously computed values of the first invariant are visualised in the deformed configuration. We remark that the onset and evolution of plastic distortions affect both quantitatively and qualitatively the time trend of pressure. Indeed, in Fig. 4, where pressure is evaluated at the midpoint of the lower boundary of the specimen, one can see that at least three facts distinguish the evolution of pressure in the poroplastic case (i.e., when remodelling occurs) from that pertaining the poroelastic one. Firstly, the maximum value of pressure attained in the absence of remodelling is much higher than the maximum reached in the presence of remodelling (it should be noticed, however, that in both cases the maxima are attained at the end of the loading ramp, i.e., at $t = 30$ s). Secondly, the rate with which the pressure tends towards the stationary state is much higher in the poroplastic case than in the poroelastic one. Thirdly, pressure seems to be a convex function of time over the interval $[0, T_0]$ in the poroelastic case, and to become concave in the poroplastic case. A possible explanation for the change of the pressure's behaviour could be given by the following argument: The pressure and the deformation are determined by the coupled equations representing the mass and linear momentum balance laws, i.e., (44a) and (44b). In particular, the balance of momentum (44b) relates the pressure, p, to the constitutive part of the first Piola-Kirchhoff stress tensor, $\boldsymbol{P}_{\mathrm{sc}}$. The plastic distortions, represented by $\boldsymbol{B}_{\mathrm{p}}$, have a direct influence on $\boldsymbol{P}_{\mathrm{sc}}$, since it holds that $\boldsymbol{P}_{\mathrm{sc}} = \hat{\boldsymbol{P}}_{\mathrm{sc}}(\boldsymbol{F}, \boldsymbol{B}_{\mathrm{p}})$, and, through the balance of momentum, they also have an indirect influence on p.

The coarsest computational grid consists of 144 prismatic elements. A regular refinement is performed three times, so that the finest grid provides 163300 degrees of freedom for the deformation and the pressure. Both the deformation, χ, and the pressure, p, are approximated by linear *ansatz* functions. As a numerical solver a Newton-method is applied. Within the Newton iteration, a Bi-CGSTAB-method, preconditioned by an ILU-decomposition, solves the linearised sub-problems. The non-linear convergence is ensured by the application of a line-search method.

6 Conclusions

In this work, we considered a biphasic, solid-fluid mixture as an idealisation of a biological system, and studied its mechanical and fluid dynamic behaviour by simulating an unconfined compression test. Our fundamental hypothesis was that the mechanical loads applied to the mixture, besides leading to a global change of shape, also induce a structural reorganisation of the solid phase, which manifests itself through plastic distortions. In order to describe this physical picture, we used the poroplastic model reported in (44a)–(44c), which results into a set of coupled, and highly non-linear equations. We recall that all our calculations have been run under the assumptions that the solid phase exhibits hyperelastic response and that the fluid obeys Darcy's law.

Equations (44a)–(44c) were solved numerically by applying a numerical procedure recently developed for monophasic continua [47], and adapted to the biphasic framework in this paper. The results of our simulations, performed with our own code, and implemented in the non-commercial software UG [96], are reported in Sect. 5. It is shown that the plastic distortions, described by $\boldsymbol{B}_{\mathrm{p}}$, influence the overall deformation, the stress distribution in the medium, and the fluid filtration velocity. This influence can be observed by comparing the results obtained in the poroplastic case with those pertaining the poroelastic one (see Figs. 3(a)–5(b)). We found that the reorganisation of the medium's internal structure has repercussions on the magnitudes of both the axial and the radial component of the Darcy's filtration velocity, which are smaller in the poroplastic case than in the poroelastic one, and has the effect of decreasing the fluid pressure as well as the magnitude of the constitutive stress in the tissue.

Our results could contribute to estimate the mechanical conditions leading to the onset of remodelling, and seem to suggest some possible consequences of the structural reorganisation of hydrated soft tissues. Moreover, they may provide indications about the mechanical conditions regulating the health of

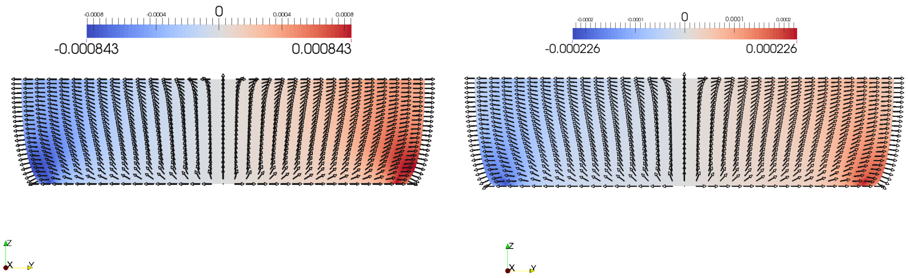

(a) Darcy's filtration velocity in radial direction [mm/s] without remodelling (left) and with remodelling (right).

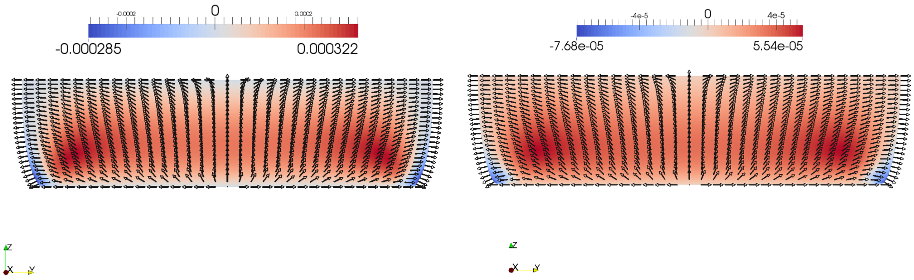

(b) Darcy's filtration velocity in axial direction [mm/s] without remodelling (left) and with remodelling (right).

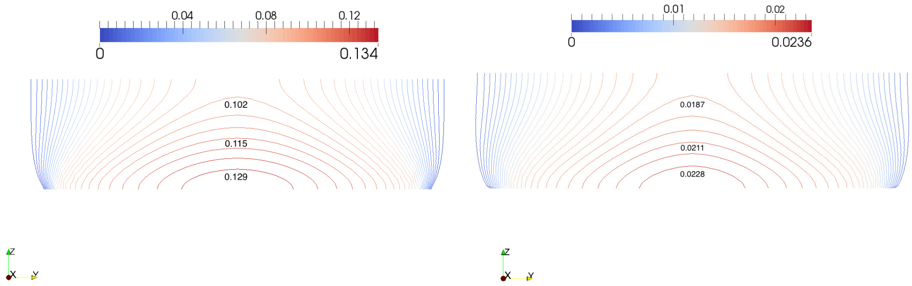

(c) Pressure isolines [N/mm^2] without remodelling (left) and with remodelling (right).

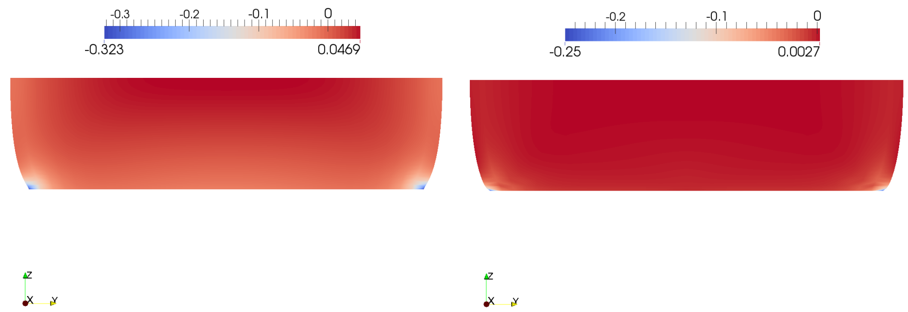

(d) First invariant of $\boldsymbol{\Sigma}_{\rm sc}$ [N/mm^2] without remodelling (left) and with remodelling (right).

Fig. 3 Comparison of the results of the unconfined compression test in the absence (left column) and in the presence (right column) of remodelling. All quantities are plotted in the deformed configuration of the sample at time $t = 30$ s

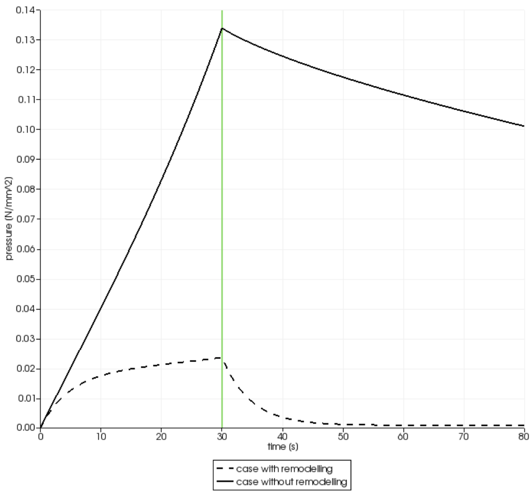

Fig. 4 Comparison of the time evolution of pressure, evaluated at the midpoint of the lower boundary of the sample, between the case without remodelling and the case with remodelling

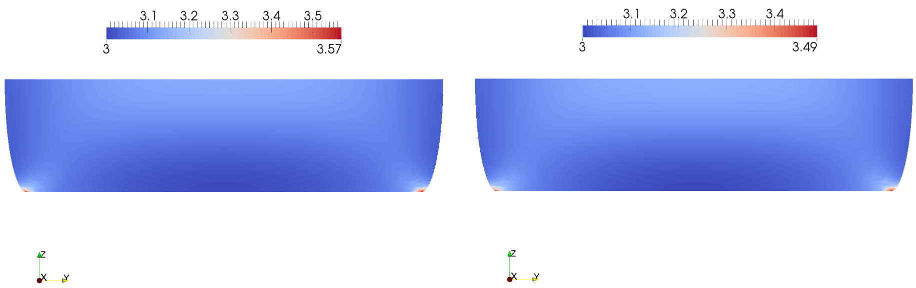

(a) First invariant of $\boldsymbol{B}_{\rm p}$ [—]

(b) Second invariant of $\boldsymbol{B}_{\rm p}$ [—]

Fig. 5 First and second invariant of $\boldsymbol{B}_{\rm p}$ in the presence of remodelling. The invariants are computed at time $t = 30$ s with respect to the reference configuration. However, in a visualisation post-process, the reference configuration is deformed by the motion map, and the invariants are visualised in the deformed configuration.

tissues. For example, in the case of articular cartilage, the health of the tissue depends on the mechanical environment in which chondrocytes live (the chondrocytes are the cells that synthesise extracellular matrix, cf. [54,55,73, 74] and references therein). Finally, the mathematical model presented in this paper could be generalised to include also growth [45] and damage [23,24,41]. Indeed, both processes have many features in common with remodelling, and can be described by extending the BKL decomposition as follows [71]

$$\boldsymbol{F} = \boldsymbol{F}_{\rm e}\boldsymbol{F}_{\rm g}\boldsymbol{F}_{\rm p}\boldsymbol{F}_{\rm d}\,, \tag{68}$$

where $\boldsymbol{F}_{\rm g}$ and $\boldsymbol{F}_{\rm d}$ denote the tensors of anelastic distortions related to growth and damage, respectively. A mathematical model based on (68) would require the introduction of two other independent evolution laws, one for $\boldsymbol{F}_{\mathrm{g}}$ and one for $\boldsymbol{F}_{\mathrm{d}}$, which would call for further adapting the numerical procedure presented in Sect. 4. This is part of our current investigations. We remark that the order with which the tensors $\boldsymbol{F}_{\mathrm{g}}$ and $\boldsymbol{F}_{\mathrm{d}}$ appear in (68) is not unique, but it becomes irrelevant if $\boldsymbol{F}_{\mathrm{g}}$ and $\boldsymbol{F}_{\mathrm{d}}$ are assumed to be purely volumetric [43].

Equations (44a) and (44b) are rather standard and constitute the starting point for both poroelastic and poroplastic models of solid-fluid mixtures. They are obtained on the basis of a series of assumptions that require: the intrinsic incompressibility of both the solid and the fluid phase, the fluid phase to be macroscopically inviscid (this implying that it can only sustain hydrostatic stresses), the hyperelastic behaviour of the solid phase, and the validity of Darcy's law. The latter involves the hydraulic conductivity tensor, which was specified in this work by means of the simplest constitutive law for isotropic materials (cf. (29a)). Although many of these hypotheses are physically sound, it could be interesting to investigate the consequences of relaxing some of them. This could lead to more general models that, on the one hand, would stimulate the development of more flexible and efficient computational algorithms, and, on the other hand, might capture some physical aspects (such as, e.g., the pore scale interactions between the solid and the fluid), which are often neglected in the standard theory.

From the computational point of view, assuming that $\boldsymbol{k}$ is proportional to $\boldsymbol{g}^{-1}$ introduces the great advantage of weakening the coupling among (44a)–(44c). Indeed, since $\boldsymbol{B}_{\mathrm{p}}$ does not feature in the mass balance law (44a), the linearisation of the functional $\mathfrak{F}_p$ needs to be performed only with respect to pressure and deformation (we recall that, actually, $\mathfrak{F}_p$ is affine in p, and that the linearisation of $\mathfrak{F}_p$ with respect to the pressure is done to get the set of equations (61a) and (61b), whose algebraic form leads to a "generalised saddle-point problem" [16,44]). In other circumstances, however, $\mathfrak{F}_p$ has to be linearised according to the same procedure as $\mathfrak{F}_\chi$. This happens, for instance, if the hydraulic conductivity is isotropic, but its constitutive expression is of the type

$$\boldsymbol{k} = \hat{\boldsymbol{k}}(\boldsymbol{F}, \boldsymbol{B}_{\mathrm{p}}) = k_0 \boldsymbol{g}^{-1} + k_1 \boldsymbol{F} \boldsymbol{B}_{\mathrm{p}} \boldsymbol{F}^{\mathrm{T}} . \tag{69}$$

In this case, indeed, the coupling among the model equations is due to both χ and $\boldsymbol{B}_{\mathrm{p}}$.

The evolution of the plastic distortions depends strongly on the physics of the anelastic phenomenon that has to be described, and, even when the "same" phenomenon is investigated, it can vary considerably depending on the accuracy of the mathematical model, on the strength of the coupling between the rate of anelastic distortions and the other variables, and on the intrinsic features of the anelastic process (which could be either rate-dependent or rate-independent, either associative or non-associative). In this paper, we chose to describe the evolution of $\boldsymbol{B}_{\mathrm{p}}$ by means of (40) because this plastic flow rule has already been successfully employed in [42] to model the reorganisation of cellular aggregates. Equation (40), however, can be generalised to include a great variety of physical situations.

The major limitation of our model is that it is isotropic and homogeneous. Indeed, both the strain energy density, $\hat{W}_{s\kappa}$, and the hydraulic conductivity, $\boldsymbol{k}$, are isotropic (see (10a) and (29a)), and all the parameters appearing in their constitutive expressions, including the referential volumetric fraction of the solid phase, ϕ_{sR}, are set equal to constants. If, on the one hand, the model could be acceptable for studying the structural evolution of tumour tissues, which are often assumed to be elastically and hydraulically isotropic [1,42,84], it fails to be accurate for tissues, such as articular cartilage, in which the presence of reinforcing collagen fibres induces anisotropy [35,78,79,94], and the constitutive laws are strongly dependent on material points. In these cases, whereas the balance laws (44a) and (44b) only need to account for the contribution of the fibres to the strain energy density and hydraulic conductivity, the plastic flow rule (44c) should be reformulated. Some of our plans for the future include the specification of the numerical techniques put forward in [39, 75] to anisotropic and inhomogeneous porous media.

One of the projects of our future research is to extend the theoretical and computational framework outlined in this paper to models accounting for phase transitions [28], to theories that describe the reorganisation of the internal structure of a body by augmenting its kinematics [21,27,45,50], and to the more general context of biomechanical models of growth and remodelling that involve, among plasticity [80], damage [81], and pre-stress effects [82], also higher order gradients of the deformation [66,67].

Acknowledgements The authors gratefully acknowledge the Polytechnic of Turin (Italy) [AG and RP], the Goethe Universität Frankfurt (Germany), the German Ministry for Economy and Technology (BMWi) —contract 02E10326 [AG and GW]— and the Baden Württemberg-Stiftung [RP]. AG thanks Melania Carfagna for useful discussions.

References

1. D. Ambrosi, F. Mollica, On the mechanics of a growing tumor, Int. J. Eng. Sci., 40, 1297–1316 (2002)
2. D. Ambrosi, L. Preziosi, On the closure of mass balance models for tumour growth, Mathematical Models and Methods in Applied Sciences, 12(5), 737–754 (2002)
3. D. Ambrosi, L. Preziosi, G. Vitale, The insight of mixtures theory for growth and remodeling, Z. Angew. Math. Phys., 61, 177–191 (2010)
4. D. Ambrosi, L. Preziosi, G. Vitale, The interplay between stress and growth in solid tumors, Mechanics Research Communications, 42, 87–91 (2012)
5. U. Andreaus, M. Colloca, D. Iacoviello, M. Pignataro, Optimal-tuning PID control of adaptive materials for structural efficiency, Struct. Multidiscip. O., 43(1), 43–59 (2011)
6. U. Andreaus, M. Colloca, D. Iacoviello. An optimal control procedure for bone adaptation under mechanical stimulus, Control Eng. Pract., 20, 575–583 (2012)
7. U. Andreaus, M. Colloca, D. Iacoviello, Modelling of trabecular architecture as result of an optimal control procedure. In: Biomedical Imaging and Computational Modeling in Biomechanics, Iacoviello D. and Andreaus U. (Eds.), Chapter II, pp. 19-37. Springer, Dordrecht, (2012)
8. U. Andreaus, M. Colloca, D. Iacoviello, Optimal bone density distributions: Numerical analysis of the osteocyte spatial influence in bone remodeling, Comput. Methods Programs Biomed., 113(1), 80–91 (2014)

9. U. Andreaus, I. Giorgio. T. Lekszycki, A 2-D continuum model of a mixture of bone tissue and bio-resorbable material for simulating mass density redistribution under load slowly variable in time, J. Appl. Math. Mech., 8, 1–23 (2013), DOI:10.1002/zamm.201200182
10. U. Andreaus, I. Giorgio, A. Madeo, The influence of different loads on the remodeling process of a bone and bioresorbable material mixture with voids, Continuum Mech. Thermodyn., Published online: 11 December 2014, DOI: 10.1007/s00161-014-0397-y
11. U.Andreaus, I. Giorgio, A. Madeo, Modeling of the interaction between bone tissue and resorbable biomaterial as linear elastic materials with voids, Z. Angew. Math. Phys., 66(1), 209–237 (2015)
12. G.A. Ateshian, On the Theory of Reactive Mixtures for Modeling Biological Growth, Biomech. Model. Mechanobiol., 6(6), 423–445 (2007)
13. G.A. Ateshian, J.A. Weiss, Anisotropic hydraulic permeability under finite deformation, Journal of Biomedical Engineering, 132, 111004-111004-7 (2010)
14. J. Bear, Dynamics of Fluids in Porous Media, Dover Publications Inc., New York (1972)
15. L.S. Bennethum, M.A. Murad, J.H. Cushman, Macroscale thermodynamics and the chemical potential for swelling porous media, Transport in Porous Media, 39, 187–225 (2000)
16. A. Benzi, G.H. Golub, J. Liesen, Numerical solution of saddle point problems, Acta Numerica, 14, 1–137 (2005)
17. D. Bigoni, D. Zaccaria, Strong ellipticity of comparison solids in elastoplasticity with volumetric non-associativity, Int. J. Solid Structures, 29(17), 2123–2136 (1992)
18. D. Bigoni, D. Zaccaria, On the eigenvalues of the acoustic tensor in elastoplasticity, European Journal of Mechanics A/Solids, 13(5), 621–638 (1994)
19. J. Bonet, R.D. Wood, Nonlinear Continuum Mechanics for Finite Element Analysis, Cambridge University Press, Cambridge, New York (2008)
20. R.M. Bowen, Compressible porous media models by use of the theory of mixtures, International Journal of Engineering Science, 20, 697–735, (1982)
21. P. Cermelli, E. Fried, S. Sellers, Configurational stress, yield and flow in rate-independent plasticity, Proc R Soc A, 457, 1447–1467 (2001)
22. S. Cleja-Tigoiu, G.A. Maugin, Eshelby's stress tensors in finite elastoplasticity, Acta Mech., 139, 231–249 (2000)
23. L. Contrafatto, M. Cuomo. A new thermodynamically consistent continuum model for hardening plasticity coupled with damage, Int J Sol Struct, 39, 6241–6271 (2002)
24. M. Cuomo, L. Contrafatto, Stress rate formulation for elastoplastic models with internal variables based on augmented Lagrangian regularisation, Int J Sol Struct, 37, 3935–3964 (2000)
25. G. Del Bufalo, L. Placidi, M. Porfiri, A mixture theory framework for modeling the mechanical actuation of ionic polymer metal composites, Smart Materials and Structures, 17(4), 1–17, ISSN: 0964-1726, doi: 10.1088/0964-1726/17/4/045010
26. F. dell'Isola, L. Rosa, C. Woźniak, Dynamics of solids with micro periodic nonconnected fluid inclusions, Archive of Applied Mechanics, 67, 215–228 (1997)
27. A. DiCarlo, S. Quiligotti, Growth and balance, Mechanics Research Communications, 29, 449–456 (2002)
28. V. Emerenyev, W. Pietraszkiewicz, The nonlinear theory of elastic shells with phase transitions, Journal of Elasticity, 85(2), 67–86 (2004)
29. M. Epstein, The Geometric Language of Continuum Mechanics. Cambridge: Cambridge University Press (2010)
30. M. Epstein, G.A. Maugin, The energy-momentum tensor and material uniformity in finite elasticity, Acta Mechanica, 83, 127–133 (1990)
31. M. Epstein, G.A. Maugin, Thermomechanics of volumetric growth in uniform bodies, Int. J. Plasticity, 16, 951–978 (2000)
32. R.A. Eve, B.D. Reddy, The variational formulation and solution of problems of finite-strain elastoplasticity based on the use of a dissipation function. Int. J. Numer. Meth. Engng., 37, 1673–1695 (1994)
33. S. Federico, Covariant Formulation of the Tensor Algebra of Non-Linear Elasticity. Int J Nonlin Mech, 47, 273–284 (2012)
34. S. Federico, Porous Materials with Statistically Oriented Reinforcing Fibres. In: Nonlinear Mechanics of Soft Fibrous Materials (CISM Courses and Lectures No. 559, International Centre for Mechanical Sciences), L. Dorfmann and R.W. Ogden (Eds.), Springer, Berling, pp. 49–120 (2015)

35. S. Federico, A. Grillo, Elasticity and permeability of porous fibre-reinforced materials under large deformations, Mechanics of Materials, 44, 58–71 (2012)
36. S. Federico, W. Herzog, On the permeability of fibre-reinforced porous materials, Int. J. Solids Struc., 45, 2160–2172 (2008)
37. S. Federico, W. Herzog, On the Anisotropy and Inhomogeneity of Permeability in Articular Cartilage, Biomech Model Mechanobiol, 7, 367–378 (2008)
38. L. Fusi, A. Farina, D. Ambrosi, Mathematical modelling of a solid-liquid mixture with mass exchange between constituents, Math. Mech. Solids, 11, 575–595 (2006).
39. G. Gabriel, K.-J. Bathe. Some Computational Issues in Large Strain Elasto-Plastic Analysis, Computers and Structures, 56(2/3), 249–267 (1995)
40. J.-F. Ganghoffer, On Eshelby tensors in the context of the thermodynamics of open systems: Application to volumetric growth, 48(12), 2081–2098 (2010)
41. T.C. Gasser, An irreversible constitutive model for fibrous soft biological tissue: A 3-D microfiber approach with demonstrative application to abdominal aortic aneurysms. Acta Biomater, 7, 2457–2466 (2011)
42. C. Giverso, L. Preziosi, Modelling the compression and reorganization of cell aggregates. Math. Med. Biol., 29, 181–204 (2012)
43. C. Giverso, M. Scianna, A. Grillo, Growing avascular tumours as elasto-plastic bodies by the theory of evolving natural configurations, Mechanics Research Communications, http://dx.doi.org/10.1016/j.mechrescom.2015.04.004. In press.
44. A. Grillo, C. Giverso, M. Favino, R. Krause, M. Lampe, G. Wittum, Mass Transport in Porous Media with Variable Mass. In: Numerical Analysis of Heat and Mass Transfer in Porous Media, Advanced Structured Materials 27, Delgado JMPQ et al. (Eds.), Springer, Berlin, Heidelberg (2012).
45. A. Grillo, S. Federico, G. Wittum, Growth, mass transfer and remodeling in fiber-reinforced, multi-constituent materials, Int J Nonlin Mech, 47, 388–401 (2012)
46. A. Grillo, A. Guaily, C. Giverso, S. Federico, Non-linear model for compression tests on articular cartilage, Journal of Biomechanical Engineering, doi: 10.1115/1.4030310. In press.
47. A. Grillo, R.-A. Prohl, G. Wittum, A generalised algorithm for anelastic processes in elastoplasticity and biomechanics. Mathematics and Mechanics of Solids. (Accepted)
48. A. Grillo, S. Federico, G. Wittum, G. Giaquinta, S. Imatani, M.V. Mićunović, Evolution of a fiber-reinforced mixture, Nuovo Cimento C, 32(1), 97–119 (2009).
49. A. Grillo, G. Wittum, G. Giaquinta, M.V. Mićunović, A multiscale analysis of growth and diffusion dynamics in biological mixtures, International Journal of Engineering Science, 47, 261–283 (2009)
50. A. Grillo, G. Wittum, A. Tomic, S. Federico, Remodelling in statistically oriented fibre-reinforced materials and biological tissues, Mathematics and Mechanics of Solids, DOI: 10.1177/1081286513515265.
51. F. Guilak, A. Ratcliffe, V.C. Mow, Chondrocyte deformation and local tissue straining articular cartilage: A confocal microscopy study, Journal of Orthopaedic Research, 13(3):410-421 (1995).
52. A. Guillou, R.W. Ogden, Growth in soft biological tissue and residual stress development, in: G.A. Holzapfel, R.W. Ogden (Eds.), Mechanics of Biological Tissue, Springer, Berlin, Heidelberg, 2006.
53. K. Hackl, F.D. Fischer, On the relation between the principle of maximum dissipation and inelastic evolution given by dissipation potentials, Proc. R. Soc. A, 464, 117–132 (2008).
54. S.-K. Han, S. Federico, A. Grillo, G. Giaquinta, W. Herzog, The mechanical behaviour of chondrocytes predicted with a micro-structural model of articular cartilage, Biomech. Model. Mechanobiol., 6(3), 139–150 (2007)
55. S.-K. Han, S. Federico, W. Herzog, A Depth-Dependent Model of the Pericellular Microenvironment of Chondrocytes in Articular Cartilage, Computer Methods in Biomechanics and Biomedical Engineering, 14 (7), 657–664 (2010), DOI: 10.1080/10255842.2010.493512
56. M.S. Hassanizadeh, Derivation of basic equations of mass transport in porous media. Part II. Generalized Darcy's and Fick's Laws, Advances in Water Resources, 9, 208–222 (1986)

57. M.H. Holmes, V.C. Mow, The nonlinear characteristics of soft gels and hydrated connective tissues in ultrafiltration, Journal of Biomechanics, 23(11), 1145–1156 (1990).
58. G.A. Holzapfel, T.C. Gasser, R.W. Ogden, A new constitutive framework for arterial wall mechanics and a comparative study of material models, Journal of Elasticity, 61, 1–48 (2000)
59. T.J.R. Hughes, The finite element method: Linear static and dynamic finite element analysis, Dover, New York, (2000)
60. T. Lekszycki, F. dell'Isola, A mixture model with evolving mass densities for describing synthesis and resorption phenomena in bones reconstructed with bio-resorbable materials, ZAMM – Journal of Applied Mathematics and Mechanics / Zeitschrift für Angewandte Mathematik und Mechanik, 6(92), 426–444 (2012)
61. Y. Liu, H. Zhang, Y. Zheng, S. Zhang, B. Chen, A nonlinear finite element model of the stress analysis of soft solids with a growing mass, Int. J. Solids Struct, 51(17), 24, 2964–2978 (2014)
62. B. Loret, F.M.F. Simões, A framework for deformation, generalized diffusion, mass transfer and growth in multi-species multi-phase biological tissues, European Journal of Mechanics A/Solids 24, 757–781 (2005)
63. V.A. Lubarda, A. Hoger, On the mechanics of solids with a growing mass, International Journal of Solids and Structures 39, 4627–4664 (2002)
64. V.A. Lubarda, Constitutive theories based on the multiplicative decomposition of deformation gradient: Thermoelasticity, elastoplasticity, and biomechanics, Appl. Mech. Rev., 57(2), 95–108 (2004)
65. J. Lubliner, Plasticity Theory, Dover Publications, Inc., Mineola, New York (2008)
66. A. Madeo, T. Lekszycki, F. dell'Isola, A continuum model for the biomechanical interactions between living tissue and bio-resorbable graft after bone reconstructive surgery, CR Mecanique, 339, 625–640 (2011)
67. A. Madeo, F. dell'Isola, F. Darve, A continuum model for deformable, second gradient porous media partially saturated with compressible fluids. J Mech Phys Sol, 61, 2196–2211 (2013)
68. J.E. Marsden, T.J.R. Hughes, Mathematical Foundations of Elasticity, Dover Publications Inc., New York (1983)
69. G.A. Maugin, M. Epstein, Geometrical Material Structure of Elastoplasticity, International Journal of Plasticity, 14(1-3), 109–115 (1998)
70. A. Menzel, A fibre reorientation model for orthotropic multiplicative growth. Configurational driving stresses, kinematics-based reorientation and algorithmic aspects. Biomechanics and Modeling Mechanobiology, 6(5), 303–320 (2007)
71. M.V. Mićunović, Thermomechanics of viscoplasticity—fundamentals and applications. Springer, Heidelberg (2009)
72. Minozzi, M., Nardinocchi, P., Teresi, L., Varano, V.: Growth-induced compatible strains. Math. Mech. Solids (2015). doi: 10.1177/1081286515570510.
73. E.K. Moo, W. Herzog, S.-K. Han, N.A. Abu Osman, B. Pingguan-Murphy, S. Federico, Mechanical Behaviour of In-Situ Chondrocytes Subjected to Different Loading Rates: A Finite Element Study, Biomechanics and Modeling in Mechanobiology, 11(7), 983–993 (2012) DOI: 10.1007/s10237-011-0367-2
74. E.K. Moo, S.-K. Han, S. Federico, A. Jinha, S. Sibole, N.A. Abu Osman, B. Pingguan-Murphy, W. Herzog, Extracellular Matrix Integrity Affects the Mechanics of In-Situ Chondrocytes under Compression, Journal of Biomechanics, 47(5), 1004–1013 (2014) DOI: 10.1016/j.jbiomech.2014.01.003
75. F.J. Montáns, K.-J. Bathe, Computational issues in large strain elasto-plasticity: an algorithm for mixed hardening and plastic spin. International Journal of Numerical Methods in Engineering, 63, 159–196 (2005)
76. B. Nedjar, On finite strain poroplasticity with reversible and irreversible porosity laws. Formulation and computational aspects, Mechanics of Materials, 68, 237–252 (2014)
77. T. Olsson, A. Klarbring, Residual stresses in soft tissue as a consequence of growth and remodelling: Application to an arterial geometry, European Journal of Mechanics A/Solids, 27, 959–974 (2008)
78. D.M. Pierce, T. Ricken, G.A. Holzapfel, A hyperelastic biphasic fibre-reinforced model of articular cartilage considering distributed collagen fibre orientations: continuum basis,

computational aspects and applications, Comput. Methods Biomech. Biomed. Eng., 16, 1344–1361 (2013)

79. D.M. Pierce, T. Ricken, G.A. Holzapfel, Modeling sample/patient-specific structural and diffusional responses of cartilage using DT-MRI. Int J Numer Methods Biomed Eng, 29, 807–821 (2013)
80. L. Placidi, A variational approach for a nonlinear one-dimensional damage-elasto-plastic second-gradient continuum model, Continuum Mechanics and Thermodynamics, ISSN: 0935-1175, doi: 10.1007/s00161-014-0405-2 (In press)
81. L. Placidi, A variational approach for a nonlinear 1-dimensional second gradient continuum damage model, Continuum Mechanics and Thermodynamics, 1–16, ISSN: 0935-1175, doi: 10.1007/s00161-14-0338-9 (2014)
82. L. Placidi, F. dell'Isola, N. Ianiro, G. Sciarra, Variational formulation of pre-stressed solid-fluid mixture theory, with an application to wave phenomena, European Journal of Mechanics, A/Solids, 27(4), 582–606 (2008)
83. S. Preston, E. Elźanowski, Material uniformity and the concept of the stress space. In: Continuous Media with Microstructure, 91–101, Springer, Heidelberg (2010)
84. L. Preziosi, D. Ambrosi, C. Verdier, An elasto-visco-plastic model of cell aggregates, Journal of Theoretical Biology, 262(1), 35–47 (2010)
85. L. Preziosi, A. Farina, On Darcy's law for growing porous media, International Journal of Non-Linear Mechanics, 37(3), 485–491 (2002)
86. L. Preziosi, G. Vitale, A multiphase model of tumour ad tissue growth including cell adhesions and plastic reorganization, Mathematical Models and Methods in Applied Science, 21, 1901–1932 (2011)
87. S. Quiligotti, On bulk growth mechanics of solid-fluid mixtures: kinematics and invariance requirements, Theor. Appl. Mech. TEOPM7, 28, 1–11 (2002)
88. S. Quiligotti, G.A. Maugin, F. dell'Isola, An Eshelbian approach to the nonlinear mechanics of constrained solid-fluid mixtures. Acta Mechanica, 160, 45–60, (2003)
89. K.R. Rajagopal, Multiple configurations in continuum mechanics, Rep. Inst. Comput. Appl. Mech, 6 (1995)
90. E.K. Rodriguez, A. Hoger, A.D. McCullogh, Stress-dependent finite growth in soft elastic tissues, Journal of Biomechanics, 27, 455–467 (1994)
91. G. Sciarra, F. dell'Isola, K. Hutter, Dilatational and compacting behavior around a cylindrical cavern leached out in a solid-fluid elastic rock salt, International Journal of Geomechanics, 5(3), 233–243 (2005)
92. J.C. Simo, A framework for finite strain elastoplasticity based on maximum plastic dissipation and the multiplicative decomposition: Part I. Continuum Formulation, Comput. Mech. Appl. M., 66, 199–219 (1988).
93. J.C. Simo, T.J.R. Hughes, Computational Plasticity, Springer, New York (1988)
94. A. Tomic, A. Grillo, S. Federico, Poroelastic materials reinforced by statistically oriented fibres—numerical implementation and application to articular cartilage. IMA Journal of Applied Mathematics, 79(5), 1017–1059 (2014) DOI:10.1093/imamat/hxu039.
95. C. Truesdell, W. Noll, The Non-Linear Field Theories of Mechanics, Handuch der Physik, III/3, Berlin: Ed. S. Flugge. Springer-Verlag.
96. A. Vogel, S. Reiter, M. Rupp, A. Nägel, G. Wittum, UG4 - A Novel Flexible Software System for Simulating PDE Based Models on High Performance Computers, Computing and Visualization in Science, DOI: 10.1007/s00791-014-0232-9 (2013)